CHINESE JOURNAL OF PHYSICS VOL. 52, NO. 1-II February 2014

Review

Nonadiabatically Coupled π-Electron Rotation and Molecular Vibration in Aromatic Molecules Excited by Polarized UV/Vis Laser Pulses

Manabu Kanno,[1] Yukari Ono,[1] Hirohiko Kono,[1] and Yuichi Fujimura[1,2]

[1]*Department of Chemistry, Graduate School of Science, Tohoku University, Sendai 980-8578, Japan*

[2]*Department of Applied Chemistry, Institute of Molecular Science and Center for Interdisciplinary Molecular Science, National Chiao-Tung University, Hsin-Chu 300, Taiwan*

(Received September 20, 2013)

We review our theoretical studies on laser-driven ultrafast π-electron rotation (ring current) and vibronically coupled molecular vibrations in aromatic molecules with quasi-degenerate excited states. The main focus of discussion is on the role of laser polarization in controlling the coherent vibronic dynamics. We first present general formulations of the coherent electronic wave packet and expectation value of electronic angular momentum for *arbitrary* laser polarization within a frozen-nuclei model. We show that the relative quantum phase of the superposed quasi-degenerate states, which determines the oscillating behavior of angular momentum, can be manipulated by the ellipticity and orientation of the incident laser. The controllability of π-electron rotation is demonstrated by electronic wave packet simulations for a model molecule. The results of nuclear wave packet simulations on effective potential energy surfaces of the molecule have revealed that the angular momentum is gradually reduced by nonadiabatic transitions. The amplitude of induced molecular vibration depends significantly on the direction of linear polarization vectors but is insensitive to the helicity of circular polarization. The characteristic feature in vibrational amplitudes is attributed to the interference between nuclear wave packets that acquire different quantum phases in nonadiabatic transition. This feature offers a new strategy for laser control of molecular vibrations through the wave packet interference in nonadiabatic transition.

DOI: 10.6122/CJP.52.617 PACS numbers: 31.50.Gh, 33.15.Bh, 82.50.Hp, 82.53.-k

I. INTRODUCTION

Continuous technological advances in optical pulse generation have been vigorously promoting applications of attosecond/several-femtosecond lasers in molecular physics, chemistry, nanoscience, etc [1]. Such ultrashort lasers instantaneously change the electronic state of molecular systems. In recent years, control and observation of ultrafast dynamics in polyatomic molecules such as valence-electron motion and molecular vibration have been attempted by means of ultrashort laser pulses. For instance, from both experimental and theoretical aspects, time-resolved photoelectron angular distribution has been utilized to monitor the ultrafast dynamics through conical intersections, e.g., in the nonadiabatic transition in nitrogen dioxide NO_2 [2], in the photodissociation of carbon disulfide CS_2 [3], and in the internal conversions of aromatic hydrocarbons [4–7]. Each of the parameters that characterize a laser pulse plays a decisive role in the excitation of molecules; the light

intensity of the pulse affects the number of molecules excited and the central frequency specifies the average energy absorbed by the molecules. The bandwidth of the incident laser is inversely proportional to the pulse duration. Among the parameters, laser polarization is attracting more and more attention as a key controlling factor of molecular motion. So far, intense polarized light pulses have been extensively employed for the alignment [8–13] and orientation [8, 11, 14–17] of molecules by manipulating their rotational states. The nonadiabatic alignment technique [12, 18], which achieves the field-free periodic alignment of linear [19–21] or nonlinear [22, 23] molecules due to their rotational revival after pulse irradiation (from several tens of femtoseconds to picoseconds), has been used in the prestage for high harmonic generation [24–26] and molecular orbital (MO) tomography [27–29].

The present state of the application of polarized lights is entering into the next stage, namely, control of vibronic dynamics in polyatomic molecules with the polarization of shorter attosecond/several-femtosecond laser fields. For C_{60} fullerene, which is a large three-dimensional π-conjugated system, Hertel *et al.* have experimentally revealed that the patterns of multiphoton ionization and subsequent fragmentation caused by an intense femtosecond near-infrared laser depend significantly on optical ellipticity [30]. They have attributed the ellipticity dependence of the ion yield to that of the two-photon absorption process to a doorway excited state of C_{60} followed by efficient multielectron dynamics.

As for theoretical work, electronic and nuclear probability density currents or fluxes in molecules triggered by polarized femtosecond lasers have been actively investigated [31–36]. Among them, we refer to the quantum simulation by Barth *et al.* of laser-driven electron ring currents in Mg porphyrin, which is a planar two-dimensional π-conjugated system, i.e., an aromatic molecule [31]. The results of the simulation performed under a frozen-nuclei condition indicated that π electrons of the molecule can be rotated along its aromatic ring by applying a circularly polarized ultraviolet (UV) laser pulse. The circular motion of π electrons around the ring is associated with the angular momentum along the molecular axis perpendicular to the ring plane. Mg porphyrin has a pair of doubly degenerate π-electronic excited states, which are the eigenstates of the electronic angular momentum with opposite signs, owing to its high molecular symmetry. On irradiation the spin angular momentum of a photon is transferred to π electrons to produce one of the eigenstates selectively, and therefore the rotation direction of π electrons is predetermined by the helicity of circular polarization. Rodriguez and Mukamel have predicted that ring currents in Mg porphyrin can be probed by circular dichroism spectroscopy [37].

Laser-induced electron dynamics in ring-shaped systems such as aromatic molecules have been reported by other authors as well [38–41]. Nobusada and Yabana have calculated electric currents and an inverse Faraday effect in cyclic Na_{10} and benzene exposed to circularly polarized laser pulses by solving the time-dependent Kohn-Sham equation in real space and real time [40]. Ulusoy and Nest have shown by optimal control simulations that the aromaticity of benzene can be switched off by exciting it to nonaromatic target states [41].

In contrast to the work by Barth *et al.*, we have demonstrated that transient rotation of π electrons in an ansa (planar-chiral) aromatic molecule can be induced along its aromatic ring by a linearly polarized UV laser pulse [42, 43]. Lowering the molecular

symmetry breaks the degeneracy of relevant excited states. In this case, the origin of directional ring current is not photon helicity but the asymmetry of the molecule. Ultrashort laser pulses can create a coherent superposition of optically-allowed quasi-degenerate excited states. The relative quantum phase of the superposed quasi-degenerate states can be controlled by the polarization direction of the incident laser with respect to the spatial configuration of the molecule. When the nonstationary electronic state is so prepared, π electrons travel in an intended direction, clockwise or counterclockwise, around the ring. Moreover, as an extension to nonadiabatic vibrational dynamics coupled to the laser-driven π-electron rotation, we have also performed nuclear wavepacket (WP) simulations including nonadiabatic interactions between quasi-degenerate excited states [44]. To the best of our knowledge, Ref. [44] is the first report on electron rotation dynamics perturbed by molecular vibrations. The amplitudes of vibronically coupled molecular vibrations in the quasi-degenerate states dramatically vary depending on the initial rotation direction of π electrons, which is determined by the linear polarization direction. We have explained this in both intuitive [45] and analytical [46, 47] ways as an interference effect between nuclear WPs ramified by nonadiabatic transition. This finding suggests that the information on attosecond π-electron dynamics can be obtained by spectroscopic detection of femtosecond molecular vibrations. Recently, we have further extended our investigation to nonadiabatic dynamics of aromatic molecules with quasi-degenerate excited states for *arbitrary* laser polarization including linear, circular, and elliptical ones [48]. The initial relative phase between the quasi-degenerate states is subject not only to the orientation of the applied laser but also to its ellipticity. It is therefore possible to create a desired superposition of the quasi-degenerate states, that is, to control π-electron rotation and vibrational amplitudes by tuning these laser parameters properly.

This article is intended to review the series of our studies on laser-driven ultrafast π-electron rotation and associated nonadiabatic couplings with molecular vibrations in aromatic molecules that have quasi-degenerate π-electronic excited states. We provide theoretical and numerical analyses in molecular optical response based on the time-dependent Schrödinger equation (TDSE) explicitly taking into account laser polarization. In Section II, we describe the concept of electronic angular momentum for aromatic molecules in terms of MO theory so as to introduce approximate angular momentum eigenstates in a quasi-degenerate system. In Section III, first, the optical excitation process of aromatic molecules is theoretically analyzed within a frozen-nuclei model to clarify the laser-polarization dependence of the relative quantum phase of the superposed quasi-degenerate states. Next, we present the numerical results of electronic WP simulations for a model system with a six-membered ring. The comparison between the excitations by linearly and circularly polarized UV laser pulses exemplifies the laser-polarization effects on π-electron rotation. In Section IV, we report the numerical results of nuclear WP simulations on effective potential energy surfaces (PESs) of the same molecule. It is shown that noticeable polarization-dependent nonadiabatic effects are found in both electronic angular momentum and vibrational amplitudes. We also discuss the laser control of the interference between the nuclear WPs of quasi-degenerate states that is caused by nonadiabatic transition. Finally, Section V concludes this article.

II. BASIC IDEA OF LASER-DRIVEN π-ELECTRON ROTATION IN AROMATIC MOLECULES

To begin with, we present the basic idea of generating ultrafast π-electron rotation in aromatic molecules by polarized lights. Because in general angular momentum serves as a measure of circular motions of a particle, introducing the concept of angular momentum eigenstates of π electrons is essential to quantify their rotation along an aromatic ring. In this section, we briefly summarize the mechanism of optically induced π-electron rotation from a viewpoint of the relationship between angular momentum eigenstates and molecular symmetry.

II-1. Angular Momentum Eigenstates: Complex and Real Orbitals

The system under consideration is an aromatic molecule of D_{Nh} symmetry and its C_N axis is chosen as the z axis. According to MO theory, complex MOs $\{|\pi_m\rangle\}$ of the molecule are given as linear combinations of atomic orbitals (LCAO-MOs) in the form [49]

$$|\pi_m\rangle = \frac{1}{N^{1/2}} \sum_{j=1}^{N} \exp\left(im\frac{2j\pi}{N}\right) |p_{zj}\rangle = \frac{1}{N^{1/2}} \sum_{j=1}^{N} \exp\left(im\phi_j\right) |p_{zj}\rangle, \tag{1}$$

where $\phi_j \equiv 2j\pi/N$ and $|p_{zj}\rangle$ denote the azimuthal angle and p_z orbital at the jth atom in the aromatic ring, respectively. The range of the integer m depends on whether N is odd or even: When N is an odd number, m reads $-(N-1)/2, \ldots, 0, \ldots (N-1)/2$ (for even N, $-N/2+1$, ..., 0, ..., $N/2$). The energy levels of $\{|\pi_m\rangle\}$ are well known as a Frost circle [50]: $|\pi_0\rangle$ is the lowest MO and, for the other values of m, $|\pi_m\rangle$ and $|\pi_{-m}\rangle$ are degenerate. For odd N, $\left|\pi_{\pm(N-1)/2}\right\rangle$ are the highest MOs; for even N, the nondegenerate $\left|\pi_{N/2}\right\rangle$ is the highest. When a molecular polygon is approximated with a complete cylindrical ring, the molecule belongs to the $D_{\infty h}$ point group and the z component of electronic angular momentum is quantized in units of the Dirac constant $\hbar$. In Eq. (1), the expansion coefficients $N^{-1/2}\exp\left(im\phi_j\right)$ have the same mathematical form as the eigenfunctions of the angular momentum operator $\hat{\ell}_z = -i\hbar\partial/\partial\phi$, $(2\pi)^{-1/2}\exp\left(im\phi\right)$, except for the normalization constant. Hence, the complex MO $|\pi_m\rangle$ can be regarded as an angular momentum eigenstate and its eigenvalue of $\hat{\ell}_z$ is $m\hbar$ for degenerate MOs or zero for nondegenerate ones.

Here, we define real MOs $|\pi_{mx}\rangle$ and $|\pi_{my}\rangle$ ($m > 0$) as linear combinations of the complex degenerate ones $|\pi_m\rangle$ and $|\pi_{-m}\rangle$:

$$|\pi_{mx}\rangle \equiv 2^{-1/2}\left(|\pi_{+m}\rangle + |\pi_{-m}\rangle\right), \tag{2a}$$

$$|\pi_{my}\rangle \equiv -2^{-1/2}i\left(|\pi_{+m}\rangle - |\pi_{-m}\rangle\right). \tag{2b}$$

From these definitions, the real MOs can be expanded in terms of $\{|p_{zj}\rangle\}$ as

$$|\pi_{mx}\rangle = \left(\frac{2}{N}\right)^{1/2} \sum_{j=1}^{N} \cos(m\phi_j)\,|p_{zj}\rangle, \tag{3a}$$

$$|\pi_{my}\rangle = \left(\frac{2}{N}\right)^{1/2} \sum_{j=1}^{N} \sin(m\phi_j)\,|p_{zj}\rangle. \tag{3b}$$

From Eqs. (2a) and (2b), we immediately obtain

$$|\pi_{\pm m}\rangle = 2^{-1/2}\left(|\pi_{mx}\rangle \pm i\,|\pi_{my}\rangle\right). \tag{4}$$

Recalling that complex AOs $|2p_{+1}\rangle$ and $|2p_{-1}\rangle$ are angular momentum eigenstates of an electron in a hydrogen atom, the relation in Eq. (4) is similar to that between the complex AOs and real ones $|2p_x\rangle$ and $|2p_y\rangle$ with the real azimuthal functions $\pi^{-1/2}\cos\phi$ and $\pi^{-1/2}\sin\phi$, respectively.

II-2. Angular Momentum Eigenstates: Perspective of Molecular Symmetry

On the basis of the concept of angular momentum eigenstates, we next explain the mechanism of π-electron rotation in Mg porphyrin interacting with a circularly polarized laser pulse [31] as an example. The symmetry of Mg porphyrin at its equilibrium geometry is D_{4h} and its highest occupied and lowest unoccupied MOs (HOMO and LUMO) are nondegenerate a_{1u} and doubly degenerate e_g orbitals, respectively [51, 52]. The degenerate LUMOs are one-electron angular momentum eigenstates with $m = \pm 1$. As for multielectron states constructed from MOs, there exist doubly degenerate ${}^1E_u$ excited states, which mainly consists of single excitations from nondegenerate MOs such as the HOMO to the LUMOs. The doubly degenerate ${}^1E_u$ states are viewed as the eigenstates of the total angular momentum operator $\hat{L}_z$ of the multielectron system with the quantum number $M = \pm 1$. We use the notations $\left|{}^1E_{u\pm}\right\rangle$ for the ${}^1E_u$ state with $M = \pm 1$. As in the case of MOs, the multielectron angular momentum eigenstates $\left|{}^1E_{u\pm}\right\rangle$ can be expressed in terms of real excited states $\left|{}^1E_{ux}\right\rangle$ and $\left|{}^1E_{uy}\right\rangle$:

$$\left|{}^1E_{u\pm}\right\rangle = 2^{-1/2}\left(\left|{}^1E_{ux}\right\rangle \pm i\left|{}^1E_{uy}\right\rangle\right). \tag{5}$$

When a circularly polarized laser pulse propagates along the C_4 axis of Mg porphyrin, either $\left|{}^1E_{u+}\right\rangle$ or $\left|{}^1E_{u-}\right\rangle$ is selected by the spin angular momentum of a photon and π electrons start to rotate clockwise or counterclockwise depending on the selected state. This is the origin of the unique correspondence between the rotation direction of π electrons and that of the polarization plane of a circularly polarized laser pulse. In this way, one finds it impossible to circulate π electrons in Mg porphyrin by a linearly polarized laser pulse, which has no spin angular momentum.

Here, let us suppose that the molecular symmetry is lowered, e.g., by introducing functional groups and/or replacing some carbon atoms in the aromatic ring with heteroatoms. For this molecule, no two-dimensional irreducible representation E is allowed

to exist and, accordingly, relevant MOs or multielectron states are not fully degenerate but quasi-degenerate. We denote the lower and higher of the quasi-degenerate excited states by $|L\rangle$ and $|H\rangle$, respectively. There exists no excited state that is an exact eigenstate of $\hat{L}_z$ in such a system. Then, how can π-electron rotation be induced in an aromatic molecule with lower symmetry? Ultrashort laser pulses can prepare a coherent superposition of the optically-allowed quasi-degenerate states. The approximate angular momentum eigenstates can be defined in analogy to Eq. (5) as

$$|\pm\rangle \equiv 2^{-1/2} \left(|L\rangle \pm i\,|H\rangle\right), \tag{6}$$

where

$$\left\langle \pm \left| \hat{L}_z \right| \pm \right\rangle \simeq \pm\hbar. \tag{7}$$

After a laser pulse prepares either $|+\rangle$ or $|-\rangle$, it subsequently evolves in time as a coherent nonstationary state because of the nonzero energy gap between the quasi-degenerate states:

$$e^{-i\hat{H}_0 t/\hbar}\,|\pm\rangle = 2^{-1/2}\left(e^{-i\omega_L t}\,|L\rangle \pm ie^{-i\omega_H t}\,|H\rangle\right) = e^{-i\omega_L t}2^{-1/2}\left(|L\rangle \pm ie^{-i2\Delta\omega t}\,|H\rangle\right), \tag{8}$$

where $\hat{H}_0$ is the field-free electronic Hamiltonian and ω_L (ω_H) is the angular frequency of $|L\rangle$ ($|H\rangle$). The energy gap is given by $2\hbar\Delta\omega \equiv \hbar(\omega_H - \omega_L)$. From Eq. (8), the approximate angular momentum eigenstates $|+\rangle$ or $|-\rangle$ can be transiently created within the period of the electronic state change, $T \equiv \pi/\Delta\omega$, except for the global phase factor $e^{-i\omega_L t}$. Therefore, transient rotation of π electrons along an aromatic ring can be achieved by selective generation of an approximate angular momentum eigenstate. The strategy for producing predominantly either $|+\rangle$ or $|-\rangle$ by a polarized laser field will be discussed in Section III.

III. LASER-POLARIZATION EFFECTS ON π-ELECTRON ROTATION

In this section, the role of laser polarization in an optical excitation of aromatic molecules with quasi-degenerate excited states is analyzed by using a three-level model. All nuclear degrees of freedom are ignored. We construct a theoretical model explicitly taking into account the polarization of an incident laser and show that the resultant superposition of the quasi-degenerate states is determined by the ellipticity and orientation of the polarization ellipse with respect to the molecule. The results of numerical electronic WP simulations in a six-membered ring molecule based on *ab initio* MO methods are also presented.

III-1. Three-Level Model Analysis

In this study, a laser field is treated classically and its spatial dependence is neglected under the dipole approximation. The time-dependent electronic Hamiltonian with a molecule-laser interaction in the length gauge is

$$\hat{H}(t) = \hat{H}_0 - \hat{\boldsymbol{\mu}} \cdot \boldsymbol{\varepsilon}(t), \tag{9}$$

where $\hat{\boldsymbol{\mu}}$ is the electric dipole moment operator and $\boldsymbol{\varepsilon}(t)$ is a laser field. The TDSE for an electronic WP is

$$i\hbar\frac{\partial}{\partial t}\left|\Psi\left(t\right)\right\rangle = \hat{H}\left(t\right)\left|\Psi\left(t\right)\right\rangle \tag{10}$$

with

$$\left|\Psi\left(0\right)\right\rangle = \left|G\right\rangle \tag{11}$$

as the initial condition, where $|G\rangle$ is the electronic ground state. To analytically solve the TDSE (10), we adopt the so-called V-type three-level model [53(a)], in which the electronic WP is expanded in terms of the minimum set, i.e., the ground and quasi-degenerate excited states:

$$\left|\Psi\left(t\right)\right\rangle = c_G\left(t\right)\left|G\right\rangle + c_L\left(t\right)e^{-i\omega_L t}\left|L\right\rangle + c_H\left(t\right)e^{-i\omega_H t}\left|H\right\rangle, \tag{12}$$

where the angular frequency of $|G\rangle$, ω_G, is set to be zero. The optically-allowed quasi-degenerate states $|L\rangle$ and $|H\rangle$ are independently coupled to $|G\rangle$, that is, $\langle L\left|\hat{\boldsymbol{\mu}}\right|H\rangle = \langle H\left|\hat{\boldsymbol{\mu}}\right|L\rangle = 0$; the other off-diagonal matrix elements of $\hat{\boldsymbol{\mu}}$ are real. For simplicity, all the diagonal elements of $\hat{\boldsymbol{\mu}}$ are assumed to be zero, which implies the presence of the inversion center in the molecule. When Eq. (12) is inserted into Eq. (10), the equation of motion for the expansion coefficient vector

$$\mathbf{C}\left(t\right) \equiv \begin{pmatrix} c_G\left(t\right) \\ c_L\left(t\right) \\ c_H\left(t\right) \end{pmatrix} \tag{13}$$

is derived as

$$\frac{d\mathbf{C}(t)}{dt} = i\begin{pmatrix} 0 & g_L(t) & g_H(t) \\ g_L\left(t\right)^* & 0 & 0 \\ g_H\left(t\right)^* & 0 & 0 \end{pmatrix}\mathbf{C}\left(t\right), \tag{14}$$

where

$$g_n\left(t\right) \equiv \frac{\langle G\left|\hat{\boldsymbol{\mu}}\right|n\rangle \cdot \boldsymbol{\varepsilon}(t)}{\hbar}e^{-i\omega_n t} \quad (n = L \text{ and } H). \tag{15}$$

From Eq. (11), at the initial time $t = 0$, $\mathbf{C}(t)$ satisfies

$$\mathbf{C}\left(0\right) = \begin{pmatrix} 1 \\ 0 \\ 0 \end{pmatrix}. \tag{16}$$

For convenience, we use the notations $\boldsymbol{\mu}_n \equiv \langle G\left|\hat{\boldsymbol{\mu}}\right|n\rangle = \langle n\left|\hat{\boldsymbol{\mu}}\right|G\rangle$. As defined in Section II-1, the z axis is perpendicular to the ring plane, which coincides with the xy plane. Both $\boldsymbol{\mu}_L$ and $\boldsymbol{\mu}_H$ lie in the xy plane [Fig. 1(a)] for $\pi\pi^*$ transitions corresponding to the excitations to

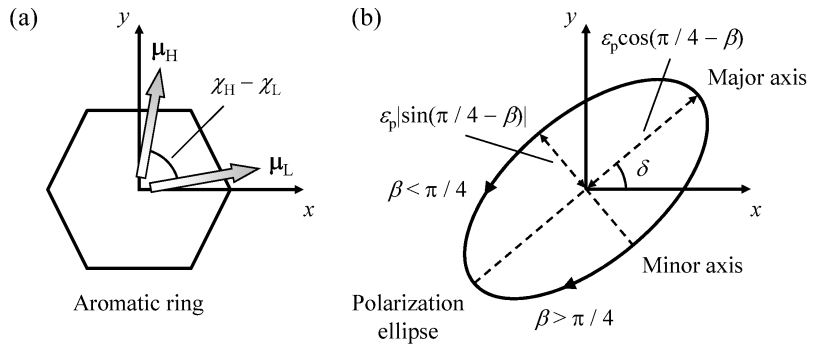

FIG. 1: (a) Spatial configurations of transition moments $\boldsymbol{\mu}_L$ and $\boldsymbol{\mu}_H$ and (b) orientation of the polarization ellipse. An aromatic molecule is represented by a hexagon. Both $\boldsymbol{\mu}_L$ and $\boldsymbol{\mu}_H$ lie in the ring plane defined as the xy plane; in a degenerate system, the x and y axes can be parallel to the directions of the transition moments. $\chi_H - \chi_L$ denotes the angle between $\boldsymbol{\mu}_L$ and $\boldsymbol{\mu}_H$. The laser field propagates in the z direction and oscillates in the xy plane. The orientation angle of the major axis of the polarization ellipse with respect to the x axis is represented by δ. The minor-to-major axial ratio is $|\tan(\pi/4 - \beta)|$.

the quasi-degenerate states. Hence, the transition electric dipole moments can be expanded as

$$\boldsymbol{\mu}_n = \mu_{nx}\mathbf{e}_x + \mu_{ny}\mathbf{e}_y \quad (n = L \text{ and } H), \tag{17}$$

where $\mathbf{e}_x$ and $\mathbf{e}_y$ are the unit vectors in the x and y directions, respectively.

The laser field is supposed to propagate in the z direction and thus $\boldsymbol{\varepsilon}(t)$ oscillates in the xy plane. The mathematical form of $\boldsymbol{\varepsilon}(t)$ is given by

$$\boldsymbol{\varepsilon}(t) = \frac{\varepsilon_p}{2} f(t) \left[e^{-i(\omega t+\varphi)}\mathbf{e} + e^{i(\omega t+\varphi)}\mathbf{e}^* \right], \tag{18}$$

where ε_p is the peak field strength, ω is the central frequency, φ is the optical phase, and $\mathbf{e}$ is the complex polarization unit vector. The time-dependent envelope function $f(t)$ varies between zero and unity for $[0, t_d]$ with t_d being the pulse duration; otherwise $f(t) = 0$. The central frequency ω is set to be resonant with the average energy of the quasi-degenerate states:

$$\omega = \omega_L + \Delta\omega = \omega_H - \Delta\omega. \tag{19}$$

The complex polarization unit vector $\mathbf{e}$ is expressed for an arbitrary polarization as

$$\mathbf{e} = e^{-i\delta}(\cos\beta)\,\mathbf{e}_{+1} + e^{i\delta}(\sin\beta)\,\mathbf{e}_{-1}, \tag{20}$$

where $\mathbf{e}_{+1}$ and $\mathbf{e}_{-1}$ are the spherical unit vectors corresponding to positive and negative helicities (spins), respectively, defined in this article as

$$\mathbf{e}_{\pm1} \equiv 2^{-12}(\mathbf{e}_x \pm i\mathbf{e}_y). \tag{21}$$

In some references the spherical unit vectors are accompanied by the signs $\mp$ before $2^{-1/2}$ but in this article the definitions in Eq. (21) are adopted. Following the convention in optics, we refer to $\mathbf{e}_{+1}$ ($\mathbf{e}_{-1}$) as left (right) circular polarization. In Eq. (20), δ represents the orientation angle of the major axis of the polarization ellipse with respect to the x axis and β is called the ellipticity angle in this article [Fig. 1(b)]. The range of β is [0, $\pi/2$] and the minor-to-major axial ratio of the polarization ellipse is equal to $|\tan(\pi/4-\beta)|$; for example, $\beta = 0$, $\pi/4$, and $\pi/2$ designate left circular, linear, and right circular polarizations, respectively. Substituting Eq. (18) into Eq. (15) yields

$$g_L(t) = \frac{f(t)}{2}\left\{\Omega_L e^{-i[(2\omega-\Delta\omega)t+\varphi]} + \Omega_L^* e^{i(\Delta\omega t+\varphi)}\right\}, \tag{22a}$$

$$g_H(t) = \frac{f(t)}{2}\left\{\Omega_H e^{-i[(2\omega+\Delta\omega)t+\varphi]} + \Omega_H^* e^{-i(\Delta\omega t-\varphi)}\right\}, \tag{22b}$$

where

$$\Omega_n \equiv \frac{\varepsilon_p}{\hbar}\boldsymbol{\mu}_n \cdot \mathbf{e} \quad (n = L \text{ and } H) \tag{23}$$

are the complex Rabi frequencies. Note that the Rabi frequencies are dependent on the polarization of the laser field, that is, on β and δ. Here, we resort to the rotating-wave approximation (RWA) [53(b)], in which the contribution of the rapidly oscillating exponentials, i.e., the first terms in Eqs. (22a) and (22b) to the time evolution of $\mathbf{C}(t)$ is averaged out and removed (since $\omega \gg \Delta\omega$). Under the RWA, Eq. (14) is rewritten as

$$\frac{d\mathbf{C}(t)}{dt} = i\frac{f(t)}{2}\begin{pmatrix} 0 & \Omega_L^* e^{i(\Delta\omega t+\varphi)} & \Omega_H^* e^{-i(\Delta\omega t-\varphi)} \\ \Omega_L e^{-i(\Delta\omega t+\varphi)} & 0 & 0 \\ \Omega_H e^{i(\Delta\omega t-\varphi)} & 0 & 0 \end{pmatrix}\mathbf{C}(t). \tag{24}$$

Even for a molecule without the inversion center, which has nonzero permanent electric dipoles, the diagonal terms in the equation of motion for $\mathbf{C}(t)$ vanish in the RWA and thereby Eq. (24) is obtained.

For the purpose of efficiently producing an approximate angular momentum eigenstate $|+\rangle$ or $|-\rangle$ defined by Eq. (6), the quasi-degenerate states $|L\rangle$ and $|H\rangle$ need to be populated equally. The laser field is therefore assumed to satisfy $|\Omega_L| = |\Omega_H|$ or, at least, $|\Omega_L| \simeq |\Omega_H|$. This leads to the orthogonality

$$\left(e^{i\theta}\boldsymbol{\mu}_L - \boldsymbol{\mu}_H\right)\cdot\mathbf{e} = 0, \tag{25}$$

where θ is the relative phase between Ω_L and Ω_H, that is,

$$\theta \equiv \arg\left(\frac{\Omega_H}{\Omega_L}\right). \tag{26}$$

When Eq. (20) is inserted into Eq. (25), the ellipticity angle β and orientation angle δ are related to the relative phase θ by

$$e^{i2\delta}\tan\beta = -\frac{\left(e^{i\theta}\boldsymbol{\mu}_L - \boldsymbol{\mu}_H\right)\cdot\mathbf{e}_{+1}}{\left(e^{i\theta}\boldsymbol{\mu}_L - \boldsymbol{\mu}_H\right)\cdot\mathbf{e}_{-1}}. \tag{27}$$

Hence, the values of β and δ that meet the condition $|\Omega_L| = |\Omega_H|$ are determined by the absolute value and argument of the right-hand side of Eq. (27), respectively. To further simplify Eq. (24), we introduce an alternative pair of superposition states

$$|S_\pm\rangle \equiv \frac{1}{\bar{\Omega}} \left(\Omega_L |L\rangle \pm \Omega_H |H\rangle\right) = \frac{\Omega_L}{\bar{\Omega}} \left(|L\rangle \pm e^{i\theta} |H\rangle\right), \tag{28}$$

where

$$\bar{\Omega} \equiv \left(|\Omega_L|^2 + |\Omega_H|^2\right)^{1/2} = 2^{1/2} |\Omega_L| = 2^{1/2} |\Omega_H| . \tag{29}$$

The superposition states in Eq. (28) are obviously normalized and the overlap between them is

$$\langle S_+ | S_- \rangle = \frac{|\Omega_L|^2 - |\Omega_H|^2}{\bar{\Omega}^2} = 0, \tag{30}$$

which proves their orthogonality. Using these superposition states, the electronic WP can be expanded as

$$|\Psi(t)\rangle = c_G(t) |G\rangle + e^{-i(\omega t+\varphi)} \left[c_+(t) |S_+\rangle + c_- (t) |S_-\rangle\right], \tag{31}$$

where

$$c_\pm (t) \equiv \frac{1}{\bar{\Omega}} \left[\Omega_L^* e^{i(\Delta\omega t+\varphi)} c_L (t) \pm \Omega_H^* e^{-i(\Delta\omega t-\varphi)} c_H (t)\right]. \tag{32}$$

Then, the time evolution of the new coefficient vector

$$\mathbf{D} (t) \equiv \begin{pmatrix} c_G (t) \\ c_+ (t) \\ c_- (t) \end{pmatrix} \tag{33}$$

obeys

$$\frac{d\mathbf{D} (t)}{dt} = \frac{i}{2} \begin{pmatrix} 0 & \bar{\Omega} f (t) & 0 \\ \bar{\Omega} f (t) & 0 & 2\Delta\omega \\ 0 & 2\Delta\omega & 0 \end{pmatrix} \mathbf{D} (t) \tag{34}$$

with the initial condition

$$\mathbf{D} (0) = \begin{pmatrix} 1 \\ 0 \\ 0 \end{pmatrix}. \tag{35}$$

III-2. Degenerate Case

Before proceeding to the solution of Eq. (34) for a quasi-degenerate system, let us consider the degenerate case of $\Delta\omega = 0$. In this case, Eq. (34) becomes extremely simple:

$$\frac{d\mathbf{D}(t)}{dt} = i\frac{\bar{\Omega}}{2} f(t) \begin{pmatrix} 0 & 1 & 0 \\ 1 & 0 & 0 \\ 0 & 0 & 0 \end{pmatrix} \mathbf{D}(t). \tag{36}$$

This clearly indicates that the system can be treated in practice as a two-level one consisting of $|G\rangle$ and $|S_+\rangle$. After integrating Eq. (36), one obtains

$$\mathbf{D}(t) = \begin{pmatrix} \cos\left[\frac{\bar{\Omega}}{2}F(t)\right] \\ i\sin\left[\frac{\bar{\Omega}}{2}F(t)\right] \\ 0 \end{pmatrix}, \tag{37}$$

where

$$F(t) \equiv \int_0^t dt' f(t'). \tag{38}$$

From Eq. (37), the system can be completely transferred from $|G\rangle$ to $|S_+\rangle$ by the so-called π pulse [53(c)], which fulfills $\bar{\Omega}F(t_d) = \pi$. When Eq. (37) is inserted into Eq. (31), the electronic WP can be written down as

$$|\Psi(t)\rangle = \cos\left[\frac{\bar{\Omega}}{2}F(t)\right]|G\rangle + i\frac{\Omega_L}{\bar{\Omega}}\sin\left[\frac{\bar{\Omega}}{2}F(t)\right] e^{-i(\omega t+\varphi)}\left(|L\rangle + e^{i\theta}|H\rangle\right). \tag{39}$$

The relative quantum phase between the degenerate excited states $|L\rangle$ and $|H\rangle$ coincides with that between the Rabi frequencies Ω_L and Ω_H, i.e., θ. Note that the relative quantum phase θ is independent of time and controllable by the ellipticity angle β and orientation angle δ. This implies that a desired superposition of the degenerate states can be created by tuning the polarization of an incident light properly. The populations of the exact angular momentum eigenstates $|+\rangle$ and $|-\rangle$, $P_\pm(t) \equiv |\langle\pm|\Psi(t)\rangle|^2$, are derived as

$$P_\pm(t) = \frac{1}{2}\sin^2\left[\frac{\bar{\Omega}}{2}F(t)\right](1 \pm \sin\theta) \tag{40}$$

and the expectation value of electronic angular momentum, $L_z(t) \equiv \left\langle \Psi(t) \left| \hat{L}_z \right| \Psi(t) \right\rangle$, is given by

$$L_z(t) = \hbar\left[P_+(t) - P_-(t)\right] = \hbar\sin^2\left[\frac{\bar{\Omega}}{2}F(t)\right]\sin\theta. \tag{41}$$

The sign of $L_z(t)$ (in other words, the rotation direction of π electrons) is determined by the relative quantum phase θ and remains unchanged throughout the time evolution: π Electrons flow in a sole direction even after a laser pulse is turned off at $t = t_d$.

Let us revert to Eq. (27), which links the relative quantum phase θ with the ellipticity angle β and orientation angle δ. For aromatic molecules with degenerate states, there are special relationships between the transition moments $\boldsymbol{\mu}_L$ and $\boldsymbol{\mu}_H$: They have the same magnitude and are perpendicular to each other, that is, $\|\boldsymbol{\mu}_L\| = \|\boldsymbol{\mu}_H\|$ and $\boldsymbol{\mu}_L \cdot \boldsymbol{\mu}_H = 0$. The x and y axes can thus be chosen to be parallel to $\boldsymbol{\mu}_L$ and $\boldsymbol{\mu}_H$, respectively, so that $\mu_{Lx} = \mu_{Hy} \neq 0$ and $\mu_{Ly} = \mu_{Hx} = 0$; in the case of Mg porphyrin, this holds when $|L\rangle = \left|{}^1E_{ux}\right\rangle$ and $|H\rangle = \left|{}^1E_{uy}\right\rangle$. Consequently, for a degenerate system, Eq. (27) is simplified as

$$e^{i2\delta} \tan\beta = -\frac{e^{i\theta} - i}{e^{i\theta} + i} = e^{i\pi/2} \tan\left[\frac{1}{2}\left(\frac{\pi}{2} - \theta\right)\right], \tag{42}$$

which involves neither transition moments nor spherical unit vectors and is purely imaginary. Given a value of β, there exist two solutions of Eq. (42):

$$\delta = \pm\frac{\pi}{4} \text{ and } \theta = \frac{\pi}{2} \mp 2\beta. \tag{43}$$

The major axis of the polarization ellipse with $\delta = \pi/4$ bisects the angle between $\boldsymbol{\mu}_L$ and $\boldsymbol{\mu}_H$ and is perpendicular to that with $\delta = -\pi/4$. In both cases, the final angular momentum $L_z(t_d)$ for the π-pulse excitation is $\hbar \sin\theta = \hbar \cos 2\beta$. In the case of circular polarization in which $\beta = 0$ or $\pi/2$, the value of δ is indeterminate from Eq. (42) or (43); in fact, it can be chosen arbitrarily as will be mentioned later.

We present illustrative examples. The case of linear polarization ($\beta = \pi/4$) is taken as the first one; Eq. (20) is then rewritten as

$$\mathbf{e} = (\cos\delta)\,\mathbf{e}_x + (\sin\delta)\,\mathbf{e}_y \tag{44}$$

and δ determines the polarization direction. The Rabi frequencies Ω_L and Ω_H are thus real-valued and their relative phase θ takes either zero or π ($e^{i\theta} = \pm 1$). Hereafter, the linear polarization vectors for $\theta = 0$ and π are denoted by $\mathbf{e}_{in}$ and $\mathbf{e}_{out}$, respectively. From Eq. (43), the values of δ for the two polarization vectors are $\delta_{in} = \pi/4$ and $\delta_{out} = -\pi/4$. As in Eq. (39), a linearly polarized laser pulse with the polarization vector $\mathbf{e}_{in}$ ($\mathbf{e}_{out}$) produces an in-phase (out-of-phase) superposition $|L\rangle + |H\rangle$ ($|L\rangle - |H\rangle$), which is an equal mixture of the exact angular momentum eigenstates $|+\rangle$ and $|-\rangle$. This leads to $P_+(t) = P_-(t)$ and thus $L_z(t) = 0$ for all t. π-Electron rotation cannot be induced in a degenerate system by a linearly polarized laser pulse.

Next, for circular polarization, $\beta = 0$ ($\pi/2$) reads

$$\mathbf{e} = e^{-i\delta}\mathbf{e}_{+1} \ (e^{i\delta}\mathbf{e}_{-1}). \tag{45}$$

When Eq. (45) is inserted into Eq. (18), the orientation angle δ is indistinguishable from the optical phase φ. Therefore, for circular polarization, δ acts as an additional optical phase and can be set to any value because Eq. (39) shows that the optical phase φ does not affect the superposition of the degenerate states. From the definition of θ in Eq. (26), we have

$$\theta = \pm(\chi_H - \chi_L) \text{ for } \mathbf{e}_{\pm 1}, \tag{46}$$

where $\chi_H - \chi_L$ is the angle between $\boldsymbol{\mu}_L$ and $\boldsymbol{\mu}_H$, that is,

$$\tan \chi_n = \frac{\mu_{ny}}{\mu_{nx}} \quad (n = L \text{ and } H). \tag{47}$$

Accordingly, $\theta = \pm\pi/2$ ($e^{i\theta} = \pm i$) in a degenerate system. The superposition states $|S_\pm\rangle$ are equivalent to the exact angular momentum eigenstates $|\pm\rangle$ ($|\mp\rangle$) for left (right) circular polarization, while the population is transferred only to $|S_+\rangle$ as in Eq. (37). π Electrons of the molecule circulate along its ring in the direction inherent to the eigenstate generated.

The above consequences for linear and circular polarizations are consistent with the discussion on laser-driven π-electron rotation in Mg porphyrin in Section II-2. The phase factor $e^{i\theta}$ yielded by elliptical polarization is neither real nor purely imaginary regardless of whether $\delta = \pm\pi/4$. As seen in Eqs. (40) and (41), the resultant behavior of π electrons is intermediate between those for linear and circular polarizations: The rotation direction of π electrons is subject to the more populated of $|+\rangle$ or $|-\rangle$, while the magnitude of $L_z(t_d)$ is less than $\hbar$ even for the π-pulse excitation.

III-3. Quasi-Degenerate Case

Now, we turn to the quasi-degenerate case of $\Delta\omega \simeq 0$. Because it is impossible to analytically integrate Eq. (34) with an arbitrary envelope function $f(t)$, we restrict $f(t)$ to a rectangular form: $f(t) = 1$ for $[0,\ t_d]$ and otherwise zero. Then, Eq. (34) becomes solvable: During irradiation,

$$\frac{d\mathbf{D}\,(t)}{dt} = \frac{i}{2}\begin{pmatrix} 0 & \bar{\Omega} & 0 \\ \bar{\Omega} & 0 & 2\Delta\omega \\ 0 & 2\Delta\omega & 0 \end{pmatrix}\mathbf{D}\,(t)\,, \tag{48}$$

of which the solution is

$$\mathbf{D}\,(t) = \begin{pmatrix} \left(\frac{\bar{\Omega}}{\Omega}\right)^2 \cos\left(\frac{\Omega}{2}t\right) + \left(\frac{2\Delta\omega}{\Omega}\right)^2 \\ i\frac{\bar{\Omega}}{\Omega}\sin\left(\frac{\Omega}{2}t\right) \\ -\frac{\bar{\Omega}(2\Delta\omega)}{\Omega^2}\left[1 - \cos\left(\frac{\Omega}{2}t\right)\right] \end{pmatrix}. \tag{49}$$

The generalized Rabi frequency

$$\Omega \equiv \left[\bar{\Omega}^2 + (2\Delta\omega)^2\right]^{1/2} \tag{50}$$

is the root-mean-square of the Rabi frequencies and the detuning frequency $2\Delta\omega$. One can readily confirm that Eq. (49) for $\Delta\omega = 0$ is identical to Eq. (37) for $f(t) = 1$. The pulse area of a laser field for a quasi-degenerate system is defined as $\Omega F(t_d)$, which is equal to Ωt_d in the rectangular-envelope case. The ground state $|G\rangle$ can be fully emptied if the rectangular-envelope pulse satisfies $2\Delta\omega \leq \bar{\Omega}$ with a pulse area of $2\arccos\left[-\left(2\Delta\omega/\bar{\Omega}\right)^2\right]$; this laser field is named the full-excitation pulse. The pulse area of the full-excitation pulse

is larger than that of the π pulse, that is, $2\arccos\left[-\left(2\Delta\omega/\bar{\Omega}\right)^2\right] > \pi$ (but not larger than 2π). Finally, we acquire the coherent electronic WP in a quasi-degenerate system:

$$|\Psi(t)\rangle = \left[\left(\frac{\bar{\Omega}}{\Omega}\right)^2 \cos\left(\frac{\Omega}{2}t\right) + \left(\frac{2\Delta\omega}{\Omega}\right)^2\right]|G\rangle + i\frac{\Omega_L}{\Omega}\alpha(t)\, e^{-i(\omega t+\varphi)}\left\{|L\rangle + e^{i[\theta-\vartheta(t)]}|H\rangle\right\}, \tag{51}$$

where

$$\alpha(t) \equiv 2\sin\left(\frac{\Omega}{4}t\right)\bar{\alpha}(t) \text{ and } \vartheta(t) \equiv 2\arg\bar{\alpha}(t) \tag{52}$$

with

$$\bar{\alpha}(t) \equiv \cos\left(\frac{\Omega}{4}t\right) + i\frac{2\Delta\omega}{\Omega}\sin\left(\frac{\Omega}{4}t\right) \tag{53}$$

The relative quantum phase between the quasi-degenerate excited states $|L\rangle$ and $|H\rangle$ is given by $\theta - \vartheta(t)$ and its temporal behavior is the main point of this model analysis. Using $\alpha(t)$ in Eq. (52), the populations $P_{\pm}(t)$ are expressed as

$$P_{\pm}(t) = \frac{1}{2}\left(\frac{\bar{\Omega}}{\Omega}\right)^2 |\alpha(t)|^2 \{1 \pm \sin[\theta - \vartheta(t)]\} \tag{54}$$

and the angular-momentum expectation value $L_z(t)$ is

$$L_z(t) = \Lambda[P_+(t) - P_-(t)] = \Lambda\left(\frac{\bar{\Omega}}{\Omega}\right)^2 |\alpha(t)|^2 \sin[\theta - \vartheta(t)], \tag{55}$$

where

$$\Lambda \equiv \left\langle + \left|\hat{L}_z\right| + \right\rangle = -\left\langle - \left|\hat{L}_z\right| - \right\rangle. \tag{56}$$

In distinction from Eq. (41), the rotation direction of π electrons can be reversed during irradiation owing to the presence of the time-dependent phase $\vartheta(t)$ in Eq. (55).

For aromatic molecules with quasi-degenerate states, Eqs. (42) and (43) do not strictly hold because in general lowering the molecular symmetry leads to $\|\boldsymbol{\mu}_L\| \neq \|\boldsymbol{\mu}_H\|$ and $\boldsymbol{\mu}_L \cdot \boldsymbol{\mu}_H \neq 0$. In this case, the linear polarization vectors $\mathbf{e}_{in}$ ($\theta = 0$) and $\mathbf{e}_{out}$ ($\theta = \pi$) can be derived by substituting Eq. (44) into Eq. (25):

$$\delta_{in,out} = \arctan\left(-\frac{\mu_{Lx} \mp \mu_{Hx}}{\mu_{Ly} \mp \mu_{Hy}}\right). \tag{57}$$

It is straightforward to find a pair of β and δ for the other values of θ from Eq. (27) with the transition moments specified. Circular polarizations do not exactly satisfy Eq. (27), i.e., the condition $|\Omega_L| = |\Omega_H|$ unless the magnitudes of $\boldsymbol{\mu}_L$ and $\boldsymbol{\mu}_H$ happen to be equal

($\|\boldsymbol{\mu}_L\| = \|\boldsymbol{\mu}_H\|$). On the assumption that the energy gap between $|L\rangle$ and $|H\rangle$ is small ($\Delta\omega \simeq 0$), the transition moments approximately fulfill $\|\boldsymbol{\mu}_L\| \simeq \|\boldsymbol{\mu}_H\|$ and/or $\boldsymbol{\mu}_L \cdot \boldsymbol{\mu}_H \simeq 0$ and accordingly the relationship among β, δ, and θ should be close to that in the degenerate case. For example, if $\|\boldsymbol{\mu}_L\| \simeq \|\boldsymbol{\mu}_H\|$, $\mathbf{e}_{in}$ and $\mathbf{e}_{out}$ whose polarization directions are defined by Eq. (57) should be almost perpendicular to each other. If also $\boldsymbol{\mu}_L \cdot \boldsymbol{\mu}_H \simeq 0$, we have $\pm i\Omega_L \simeq \Omega_H$ ($\theta \simeq \pm\pi/2$) for $\mathbf{e}_{\pm 1}$.

The time-dependent part of the relative quantum phase, i.e., $\vartheta(t)$ follows

$$\tan\left[\frac{\vartheta(t)}{2}\right] = \frac{2\Delta\omega}{\Omega}\tan\left(\frac{\Omega}{4}t\right) \tag{58}$$

from Eqs. (52) and (53). Hence, $\vartheta(t)$ changes temporally as $0 \to \pi/2 \to \pi \to 3\pi/2 \to 2\pi \to \ldots$ with the progression of time, $0 \to T_R - \gamma \to T_R \to T_R + \gamma \to 2T_R \to \ldots$, where $T_R \equiv 2\pi/\Omega$ is the period of the (generalized) Rabi oscillations and $\gamma \equiv 4\arctan(2\Delta\omega/\Omega)/\Omega$. Because $2\Delta\omega \leq \Omega$, T_R is not larger than the period T of the field-free electronic state change and $\gamma \leq T_R/2$. The relative quantum phase grows from its initial value θ in the negative direction by $\vartheta(t)$; if the full-excitation pulse is employed, $\vartheta(t_d) \leq \pi$ from the inequality $T_R/2 < 2\arccos\left[-\left(2\Delta\omega/\bar{\Omega}\right)^2\right]/\Omega \leq T_R$. The populations $P_{\pm}(t)$ and the expectation value $L_z(t)$ vary in time according to the relative quantum phase $\theta - \vartheta(t)$ as shown in Eqs. (54) and (55), respectively.

After the end of a laser pulse at $t = t_d$, the electronic WP propagates freely. In a similar fashion to Eq. (8), the relative quantum phase in the free propagation is $\theta - \vartheta(t_d) - 2\Delta\omega(t - t_d)$ and thereby the coherent superposition of the quasi-degenerate states oscillates with the period T. Eventually, the populations $P_{\pm}(t)$ and the expectation value $L_z(t)$ for $t > t_d$ are also the oscillating functions of t in the form

$$P_{\pm}(t) = \frac{1}{2}\left(\frac{\bar{\Omega}}{\Omega}\right)^2 |\alpha(t_d)|^2 \{1 \pm \sin[\theta - \vartheta(t_d) - 2\Delta\omega(t - t_d)]\} \tag{59}$$

and

$$L_z(t) = \Lambda\left(\frac{\bar{\Omega}}{\Omega}\right)^2 |\alpha(t_d)|^2 \sin[\theta - \vartheta(t_d) - 2\Delta\omega(t - t_d)], \tag{60}$$

respectively. The approximate angular momentum eigenstates $|+\rangle$ and $|-\rangle$ are alternately generated as predicted in Section II-2 and therefore the rotation direction of π electrons switches between clockwise and counterclockwise. This is a notable difference from the degenerate case, in which the rotation direction is fixed and the angular-momentum expectation value $L_z(t)$ is constant after the applied pulse fully decays.

We have formulated the coherent electronic WP $|\Psi(t)\rangle$ and the angular-momentum expectation value $L_z(t)$ of aromatic molecules with quasi-degenerate excited states irradiated by a laser pulse of arbitrary polarization. It should be emphasized that, despite the subsequent oscillating behavior, the initial relative phase of the superposed quasi-degenerate states or the initial rotation direction of π electrons depends on the relative phase between

the Rabi frequencies, θ, which is defined by Eq. (26) and can be manipulated by the ellipticity angle β and orientation angle δ of the incident laser. Generation of polarization-shaped femtosecond UV laser pulses has become experimentally realizable [54, 55]. The efficient scheme for production of circularly polarized attosecond extreme UV laser pulses has been theoretically proposed [56]. In Section III-4, comparison will be made between this theoretical analysis in the rectangular-envelope case and numerical electronic WP simulations for pulse excitation with smooth rise and decay.

III-4. Numerical Demonstration for a Six-Membered Ring Molecule

We present the numerical results of electronic WP simulations for an aromatic molecule with a six-membered ring, 2,5-dichloropyrazine (DCP), of which the molecular formula is illustrated in Fig. 2(a). All *ab initio* electronic structure computations in this article were performed with the 6-31G* Gaussian basis set [57] by using the quantum chemistry program MOLPRO [58]. The geometry of DCP was optimized in the ground state at the level of the second-order Møller-Plesset perturbation theory (MP2) [57] and the optimized geometry was of C_{2h} symmetry. Then, to evaluate the excited-state properties at this geometry, the single-point ground- and excited-state calculation was executed at the state-averaged complete-active-space self-consistent field (CASSCF) [57] level of theory with ten active electrons and eight active (four a_u and four b_g) orbitals [abbreviated as CASSCF(10,8)]. At the optimized geometry in the ground state $|G\rangle = \left|1^1A_g\right\rangle$, DCP has a pair of optically-allowed quasi-degenerate excited states, $|L\rangle = \left|3^1B_u\right\rangle$ and $|H\rangle = \left|4^1B_u\right\rangle$, with the energy gap $2\hbar\Delta\omega = 0.44$ eV (Table I). As presented in Table I, the magnitudes of the transition electric dipole moments between the ground and two excited states, $\boldsymbol{\mu}_L$ and $\boldsymbol{\mu}_H$, are $1.66ea_0$ and $1.58ea_0$, respectively, where e is the elementary charge and a_0 is the Bohr radius; these values ensure $\|\boldsymbol{\mu}_L\| \simeq \|\boldsymbol{\mu}_H\|$. The directions of $\boldsymbol{\mu}_L$ and $\boldsymbol{\mu}_H$ are depicted in Fig. 2(b). The angle between them is $\chi_H - \chi_L = 0.35\pi$, which is smaller than $\pi/2$ in the degenerate case. The approximate angular momentum eigenstates $|+\rangle$ and $|-\rangle$ in DCP are superpositions of $|L\rangle$ and $|H\rangle$ as in Eq. (6), where $\Lambda = 0.98\hbar$. π Electrons with positive (negative) angular momentum travel counterclockwise (clockwise) around the ring in Fig. 2(a).

To elucidate the effects of laser polarization on π-electron rotation, we compare the results of electronic WP simulations for linear ($\beta = \pi/4$) and circular ($\beta = 0$ and $\pi/2$) polarizations. The orientation angles δ of the linear polarization vectors $\mathbf{e}_{in}$ and $\mathbf{e}_{out}$ were evaluated from Eq. (57) [Fig. 2(b)]; the two polarization vectors are almost perpendicular with an angle of 0.48π as expected from $\|\boldsymbol{\mu}_L\| \simeq \|\boldsymbol{\mu}_H\|$. For circular polarizations ($\mathbf{e}_{+1}$ and $\mathbf{e}_{-1}$), we set $\delta = 0$. The excitations by a laser pulse $\boldsymbol{\varepsilon}(t)$ with the four different polarization vectors are termed $\mathbf{e}_{in}$, $\mathbf{e}_{out}$, $\mathbf{e}_{+1}$, and $\mathbf{e}_{-1}$ excitations. Instead of the rectangular function adopted in the model analysis in Section III-3, we here assumed a $\sin^2$ envelope:

$$f(t) = \sin^2\left(\frac{\pi t}{t_d}\right) \text{ for } [0, t_d] \tag{61}$$

and otherwise zero. The central frequency ω was determined from Eq. (19) with the energies in Table I: $\omega = 9.62$ eV$/\hbar$ (corresponding to the wavelength of 129 nm). The other common

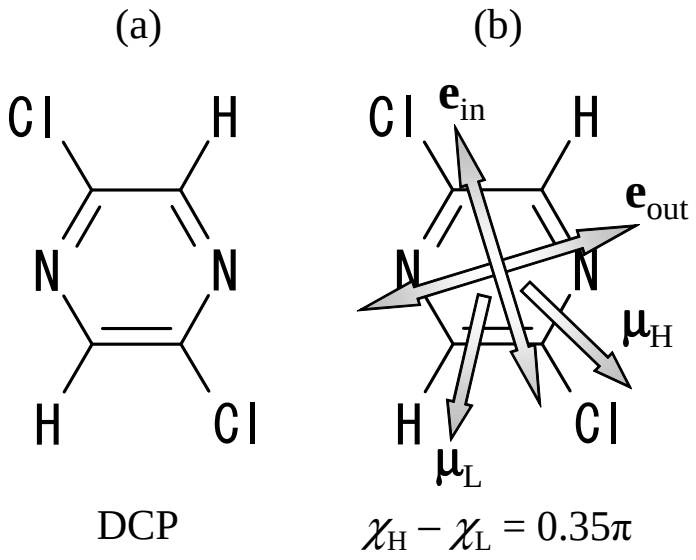

FIG. 2: (a) Molecular formula of DCP. (b) Directions of transition moments $\boldsymbol{\mu}_L$ and $\boldsymbol{\mu}_H$ at the ground-state optimized geometry of DCP as well as those of linear polarization vectors $\mathbf{e}_{in}$ and $\mathbf{e}_{out}$ whose orientation angles are defined by Eq. (51). The angle between $\boldsymbol{\mu}_L$ and $\boldsymbol{\mu}_H$ is 0.35π and that between $\mathbf{e}_{in}$ and $\mathbf{e}_{out}$ is 0.48π.

TABLE I: Properties of optically-allowed π-electronic excited states of DCP. The excited states whose transition energies from the ground state $|G\rangle = \left|1^1A_g\right\rangle$ are less than 10.0 eV are listed. The magnitudes of the transition moments between $|G\rangle$ and the respective excited states are also presented. The *ab initio* geometry optimization for $|G\rangle$ and succeeding single-point calculation were carried out at the MP2/6-31G* and CASSCF(10,8)/6-31G* levels of theory, respectively.

Excited state	Transition energy (eV)	Magnitude of transition moment (ea_0)
$\left\|4^1B_u\right\rangle$	9.84	1.58
$\left\|3^1B_u\right\rangle$	9.40	1.66
$\left\|2^1B_u\right\rangle$	8.04	1.49
$\left\|1^1B_u\right\rangle$	4.78	0.70

laser parameters for the four types of excitations were $t_d = 7.26$ fs and $\varphi = 0$. In analogy to the full-excitation pulse in the rectangular-envelope case, the peak field strength ε_p was set so that the pulse area $\Omega F(t_d)$, which is equal to $\Omega t_d/2$ for a $\sin^2$ envelope, was $2\arccos\left[-\left(2\Delta\omega/\bar{\Omega}\right)^2\right]$ with $2\Delta\omega \leq \bar{\Omega}$. The Rabi frequencies to meet this requirement for $t_d = 7.26$ fs were $\bar{\Omega} = 0.62$ eV/$\hbar$ and $\Omega = 0.76$ eV/$\hbar$. The values of ε_p determined from the Rabi frequencies for $\mathbf{e}_{in}$, $\mathbf{e}_{out}$, $\mathbf{e}_{+1}$, and $\mathbf{e}_{-1}$ excitations were 5.99, 9.80, 7.22, and 7.22

GVm^{-1}, respectively. Because we have $\|\boldsymbol{\mu}_L\| \simeq \|\boldsymbol{\mu}_H\|$ for DCP, the condition $|\Omega_L| \simeq |\Omega_H|$ (but not $\pm i\Omega_L \simeq \Omega_H$) approximately holds for circular polarizations. For the four types of excitations, we numerically solved Eqs. (14) and (15) without the RWA by the Runge-Kutta method. The time step for the numerical integration was 0.0024 fs (2.4 as).

Figure 3 shows the expectation value of electronic angular momentum $L_z(t)$ for the four types of excitations as a function of time. In the course of the interaction with the laser pulse $\boldsymbol{\varepsilon}(t)$, the timing of the initial increase in the magnitude of $L_z(t)$ and its sign (i.e., the phase in the oscillation of angular momentum) evidently depend on the type of excitation. In Fig. 3(a), the temporal behaviors of $L_z(t)$ for $\mathbf{e}_{in}$ and $\mathbf{e}_{out}$ excitations are identical except for opposite signs: For $\mathbf{e}_{in}$ ($\mathbf{e}_{out}$) excitation, π electrons start to rotate clockwise (counterclockwise), while in both cases the amplitude of $L_z(t)$ reaches almost $\hbar$ at $t = 5.4$ fs, which is designated by the vertical broken line in Fig. 3(a). This agrees with the difference in the initial relative phase θ by π between the two linear polarization vectors predicted in the model analysis. Compared to $\mathbf{e}_{in}$ and $\mathbf{e}_{out}$ excitations, the magnitudes of $L_z(t)$ for circular polarizations in Fig. 3(b) grow earlier. In addition, a peak of angular momentum for $\mathbf{e}_{+1}$ ($\mathbf{e}_{-1}$) excitation indicated by the vertical broken lines in Fig. 3(b) appears 1.6 fs later (1.0 fs earlier) than those at $t = 5.4$ fs in Fig. 3(a). Although there is a small difference between the time intervals 1.6 and 1.0 fs due to the relatively slow rise of the $\sin^2$ envelope, the peak positions of $L_z(t)$ in Fig. 3(b), which oscillate with different phases from those for linear polarizations, are fairly consistent with $\theta = \pm\,(\chi_H - \chi_L) = \pm 0.35\pi$ for $\mathbf{e}_{\pm 1}$. These agreements with the model analysis manifest the controllability of the initial relative phase of the superposed quasi-degenerate states by laser polarization. As in Eq. (55), the magnitude of $L_z(t)$ turns to decrease or even the rotation direction of π electrons flips before the laser pulse ceases at $t = t_d = 7.26$ fs. Finally, the total population in the quasi-degenerate states reaches 0.995 and thus the amplitude of $L_z(t)$ achieves $0.97\hbar$ for all the four types of excitations. This indicates that a smoothly rising and decaying pulse with a pulse area of $2\arccos\left[-\left(2\Delta\omega/\bar{\Omega}\right)^2\right]$ can excite almost all the population in $|G\rangle$ as does the full-excitation pulse in the rectangular-envelope case. After irradiation, the angular momentum oscillates with the period of $T = \pi/\Delta\omega = 9.4$ fs as in Eq. (60).

High-intensity UV lights such as used for the simulations in Fig. 3 may induce two-photon excitations to higher excited states or ionizations but the contribution of these additional processes is not large [42, 45, 47]. The use of weaker laser pulses does not affect the conclusions of this article, although less population is transferred to the quasi-degenerate excited states.

IV. LASER-POLARIZATION EFFECTS ON NONADIABATICALLY COUPLED VIBRONIC DYNAMICS

In Section III, we theoretically and numerically examined the effects of laser polarization on π-electron rotation under the frozen-nuclei condition. Without nuclear motions, ring currents should continue flowing (oscillating) even after the end of a laser pulse until a spontaneous emission relaxes the molecule. However, nonadiabatic couplings with molec-

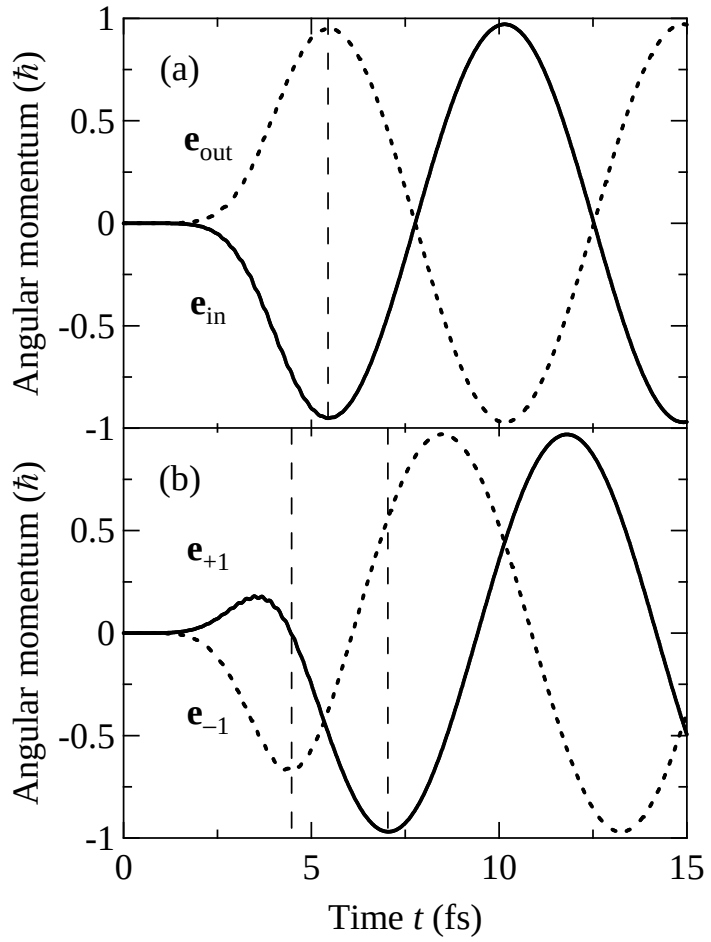

FIG. 3: Expectation value of the electronic angular momentum $L_z(t)$ in DCP irradiated by (a) linearly and (b) circularly polarized UV laser pulses calculated from electronic WP simulations at the optimized geometry of $|G\rangle$. In panel (a), the expectation values for $\mathbf{e}_{in}$ and $\mathbf{e}_{out}$ excitations are denoted by the solid and dotted lines, respectively. The peaks at $t = 5.4$ fs are indicated by the vertical broken line. In panel (b), the expectation values for $\mathbf{e}_{+1}$ and $\mathbf{e}_{-1}$ excitations are denoted by the solid and dotted lines, respectively. The peaks at $t = 4.5$ and 7.0 fs are indicated by the vertical broken lines. The laser pulses fully decay at $t = 7.26$ fs.

ular vibrations need to be considered to reveal the actual duration of π-electron rotation. It should also be clarified how the polarization of the applied laser influences vibrational motions of the molecule through π-electron rotation. In this section, we report the results of nuclear WP simulations on effective PESs with respect to selected vibrational modes of the same molecule DCP. The molecule is assumed to be preoriented, e.g., by the nonadiabatic optical alignment technique [12, 18].

IV-1. Effective Potential Energy Surfaces

To select the effective vibrational degrees of freedom for nuclear WP simulations, the geometry of DCP was optimized in the quasi-degenerate excited states $|L\rangle$ and $|H\rangle$ at the CASSCF(10,8) level of theory. The optimized geometries of both $|L\rangle$ and $|H\rangle$ also belong to the C_{2h} point group. Hence, the displacements from the optimized geometry of $|G\rangle$ to that of $|L\rangle$ and $|H\rangle$ are totally symmetric. Furthermore, vibrational modes that nonadiabatically couple two ^1B_u states $|L\rangle$ and $|H\rangle$ are totally symmetric A_g modes as well. For these reasons, we consider two types of A_g normal modes with large potential displacements and nonadiabatic coupling matrix element between $|L\rangle$ and $|H\rangle$, namely, breathing and distortion modes of which the vibrational vectors are illustrated in Fig. 4. The harmonic wave numbers of the breathing and distortion modes in $|G\rangle$ are 1160 and 1570 cm^{-1}, respectively. Nonadiabatic couplings between the ground and two excited states were neglected because $|L\rangle$ and $|H\rangle$ lie far above $|G\rangle$ and there is no potential crossing between them near the Franck-Condon region. The two-dimensional adiabatic PESs of $|L\rangle$ and $|H\rangle$ with respect to the normal coordinates of the breathing and distortion modes were calculated at the CASSCF(10,8) level of theory (Fig. 5). There exists an avoided crossing (not a conical intersection) between the PESs, although whether it is an avoided crossing or a conical intersection does not influence the qualitative discussion below. At the crossing point, the two PESs are separated by about 190 cm^{-1}. We performed a calculation at the level of the second-order CAS perturbation theory (CASPT2) [57] and confirmed that the position of the avoided crossing remains unchanged when dynamical electron correlation is taken into account, while the PESs are lowered by ~ 3 eV.

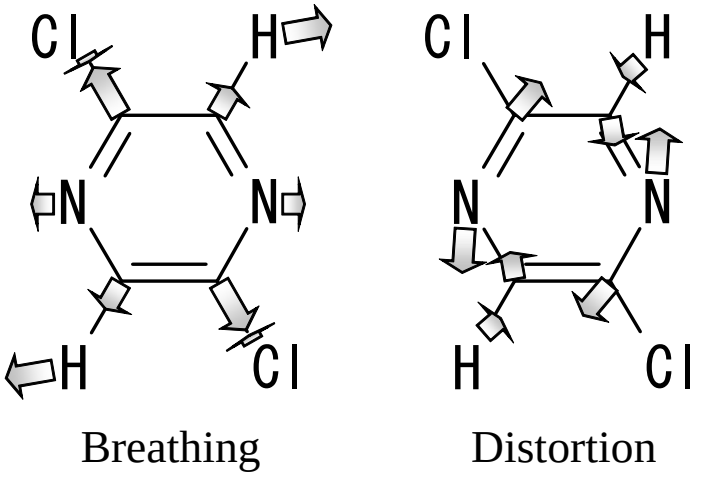

FIG. 4: Effective vibrational modes of DCP. Normal mode vectors of the breathing and distortion-modes are represented by arrows.

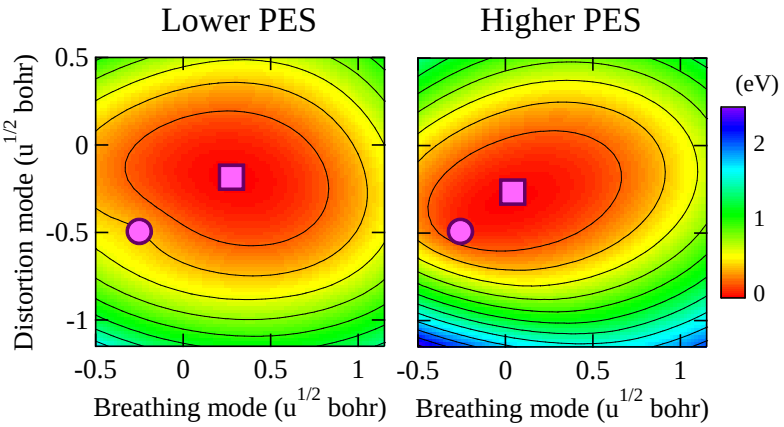

FIG. 5: Two-dimensional adiabatic PESs of $|L\rangle$ and $|H\rangle$ with respect to the breathing and distortion modes of DCP. The origin of the PESs is the optimized geometry of $|G\rangle$. The minimum of each PES and the avoided crossing between them are designated by a square and circle, respectively.

IV-2. Propagation of Nuclear Wave Packets

We describe the method of real-time nuclear WP propagation for nonadiabatically coupled vibronic dynamics. The initial nuclear WP is set to be the wave function of the vibrational ground state $(v_b,\, v_d) = (0,\, 0)$ in $|G\rangle$, where v_b and v_d designate the vibrational quantum numbers of the breathing and distortion modes, respectively. The system is then electronically excited by a laser pulse $\boldsymbol{\varepsilon}(t)$ of the form in Eq. (18). If the state vector of the system is expanded in terms of the three adiabatic states $\{|n\rangle;\ n = G,\ L,\ \text{and}\ H\}$, the time evolution of the expansion coefficients $\psi_n(\mathbf{Q}, t)$, where $\mathbf{Q}$ is the mass-weighted nuclear position or vibrational mode vector, can be obtained, in principle, from the following equations of motion [59]:

$$i\hbar\frac{\partial}{\partial t}\psi_n(\mathbf{Q},t) = \left[-\frac{\hbar^2}{2}\nabla^2 + V_n(\mathbf{Q})\right]\psi_n(\mathbf{Q},t) + \sum_{n'}\left[G_{nn'}(\mathbf{Q}) - \boldsymbol{\mu}_{nn'}(\mathbf{Q})\cdot\boldsymbol{\varepsilon}(t)\right]\psi_{n'}(\mathbf{Q},t), \tag{62}$$

where ∇ is the nabla with respect to $\mathbf{Q}$. $V_n(\mathbf{Q})$ are the adiabatic potentials and $G_{nn'}(\mathbf{Q})$ are the nonadiabatic terms defined as

$$G_{nn'}(\mathbf{Q}) \equiv -\frac{\hbar^2}{2}\left(\langle n|\nabla^2 n'\rangle + 2\langle n|\nabla n'\rangle\cdot\nabla\right). \tag{63}$$

Nevertheless, in practice, it is difficult to evaluate the nonadiabatic terms $G_{nn'}(\mathbf{Q})$. An alternative approach is needed to include the effects of nonadiabatic couplings on nuclear WP propagation.

To avoid the above-mentioned problem inherent in the adiabatic representation, we take advantage of the diabatic one. Rigorous construction of the adiabatic-diabatic unitary

transformation matrix requires the derivative coupling matrix $\langle n|\nabla n'\rangle$ [60, 61], which is, as noted above, difficult to compute. Instead, we utilize the quasi-diabatization scheme proposed by Simah *et al.* [62] that is based on an analysis of configuration interaction vectors; it has been implemented by the original authors in MOLPRO. We expanded the state vector of the system in terms of the three diabatic states $\left\{\left|n^D\right\rangle\right\}$, each of which is a linear combination of the adiabatic states $|G\rangle$, $|L\rangle$, and $|H\rangle$. The diabatic WPs $\psi_n^D(\mathbf{Q},t)$ (expansion coefficients for $\left|n^D\right\rangle$) can be propagated by solving the coupled equations [59]

$$i\hbar\frac{\partial}{\partial t}\psi_n^D(\mathbf{Q},t) = -\frac{\hbar^2}{2}\nabla^2\psi_n^D(\mathbf{Q},t) + \sum_{n'}\left[V_{nn'}^D(\mathbf{Q}) - \boldsymbol{\mu}_{nn'}^D(\mathbf{Q})\cdot\boldsymbol{\varepsilon}(t)\right]\psi_{n'}^D(\mathbf{Q},t), \quad (64)$$

where $V_{nn'}^D(\mathbf{Q})$ are the diabatic potentials ($n = n'$) and couplings ($n \neq n'$) and $\boldsymbol{\mu}_{nn'}^D(\mathbf{Q})$ are the transition moments between the two diabatic states. The coupled equations can be integrated numerically with the split-operator method for a multisurface Hamiltonian [63]. The resultant diabatic WPs $\psi_n^D(\mathbf{Q},t)$ are converted to adiabatic WPs $\psi_n(\mathbf{Q},t)$.

The split-operator integration of Eq. (64) was executed with the aid of the fast Fourier transform algorithm. For each of the two modes, the domain $[-1.60\ \mathrm{u}^{1/2}a_0,\ 1.55\ \mathrm{u}^{1/2}a_0]$ with u being the unified atomic mass unit was divided into 64 grid points at intervals of $0.05\ \mathrm{u}^{1/2}a_0$ so as to represent nuclear WPs. The time step for the WP propagation was 0.0024 fs (2.4 as).

IV-3. Nonadiabatic Population Transfer

Figure 6 shows the temporal change in the populations of the quasi-degenerate states $|L\rangle$ and $|H\rangle$ for $\mathbf{e}_{in}$, $\mathbf{e}_{out}$, $\mathbf{e}_{+1}$, and $\mathbf{e}_{-1}$ excitations. The laser pulses for the four types of excitations were the same as used for the frozen-nuclei simulations in Fig. 3. The populations on the two adiabatic PESs are defined as

$$P_n(t) \equiv \int d\mathbf{Q}\,|\psi_n(\mathbf{Q},t)|^2 \quad (n = L \text{ and } H). \quad (65)$$

In all the four cases, a significant amount of the population is transferred to the quasi-degenerate states and divided almost equally between them at $t < 4$ fs. When the laser pulse vanishes at $t = t_d = 7.26$ fs, the total population in the quasi-degenerate states, $P_L(t_d) + P_H(t_d)$, reaches 0.84, 0.93, 0.89, and 0.91 for $\mathbf{e}_{in}$, $\mathbf{e}_{out}$, $\mathbf{e}_{+1}$, and $\mathbf{e}_{-1}$ excitations, respectively. The polarization-dependent reductions in $P_L(t_d) + P_H(t_d)$ from those under the frozen-nuclei condition (0.995) are ascribed to the coordinate dependence of $\boldsymbol{\mu}_L(\mathbf{Q})$ and $\boldsymbol{\mu}_H(\mathbf{Q})$ in the Franck-Condon region because the laser pulses were designed with the transition moments at the optimized geometry of $|G\rangle$ as described in Section III-4.

The subsequent behaviors of $P_L(t)$ and $P_H(t)$ are entirely different among the four types of excitations. For $\mathbf{e}_{in}$ excitation [Fig. 6(a)], a small fraction of the population shifts from $|L\rangle$ to $|H\rangle$ by $t \sim 10$ fs and then a downward population transfer takes place around $t \sim$ 10–14 fs by nonadiabatic transition. In the case of $\mathbf{e}_{out}$ [Fig. 6(b)], a considerable amount of the population is transferred from $|H\rangle$ to $|L\rangle$ and consequently $P_L(t)$ is more than seven-times larger than $P_H(t)$ at $t \sim 10$ fs. Afterwards, the direction of population

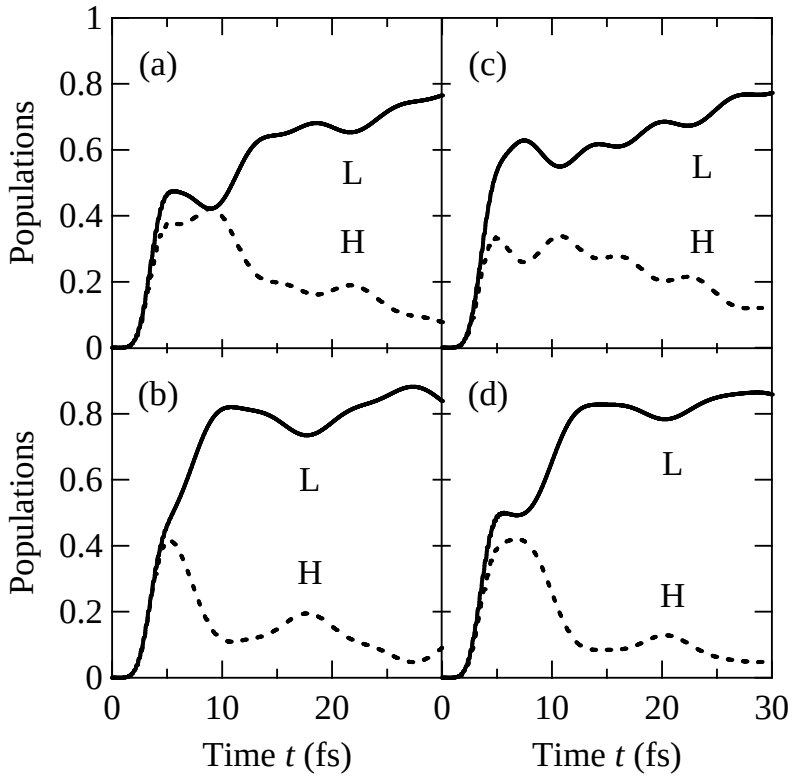

FIG. 6: Temporal behavior in the populations of the quasi-degenerate excited states for (a) $\mathbf{e}_{in}$, (b) $\mathbf{e}_{out}$, (c) $\mathbf{e}_{+1}$, and (d) $\mathbf{e}_{-1}$ excitations calculated from nuclear WP simulations. In each panel, the populations of $|L\rangle$ and $|H\rangle$ are denoted by the solid and dotted lines, respectively. The laser pulses fully decay at $t = 7.26$ fs.

transfer is reversed periodically with the rather small portion of the population transferred. In contrast, the nonadiabatic transition for $\mathbf{e}_{+1}$ excitation persists much longer [Fig. 6(c)]: A part of the population is continuously exchanged between the quasi-degenerate states and thus electronic relaxation is completed after $t = 30$ fs. In the remaining case, i.e., $\mathbf{e}_{-1}$ excitation [Fig. 6(d)], the behaviors of $P_L(t)$ and $P_H(t)$ are more or less intermediate between those for $\mathbf{e}_{in}$ and $\mathbf{e}_{out}$ excitations: A substantial population transfer from $|H\rangle$ to $|L\rangle$ is observed around $t \sim 8$–13 fs. These distinct patterns in the evolutions of $P_L(t)$ and $P_H(t)$ will be explained in Section IV-6. The results in Fig. 6 indicate that the polarization of the applied laser exerts a profound influence on the nonadiabatic transition between the quasi-degenerate states, which occurs mainly after irradiation.

IV-4. Electronic Angular Momentum and Vibrational Spectrum

The expectation value of electronic angular momentum $L_z(t)$ for the four types of excitations are plotted as a function of time in Fig. 7. For both linear and circular polarizations, the behavior of $L_z(t)$ is similar to that in Fig. 3 while $P_L(t) \simeq P_H(t)$ ($t < 4$ fs) except

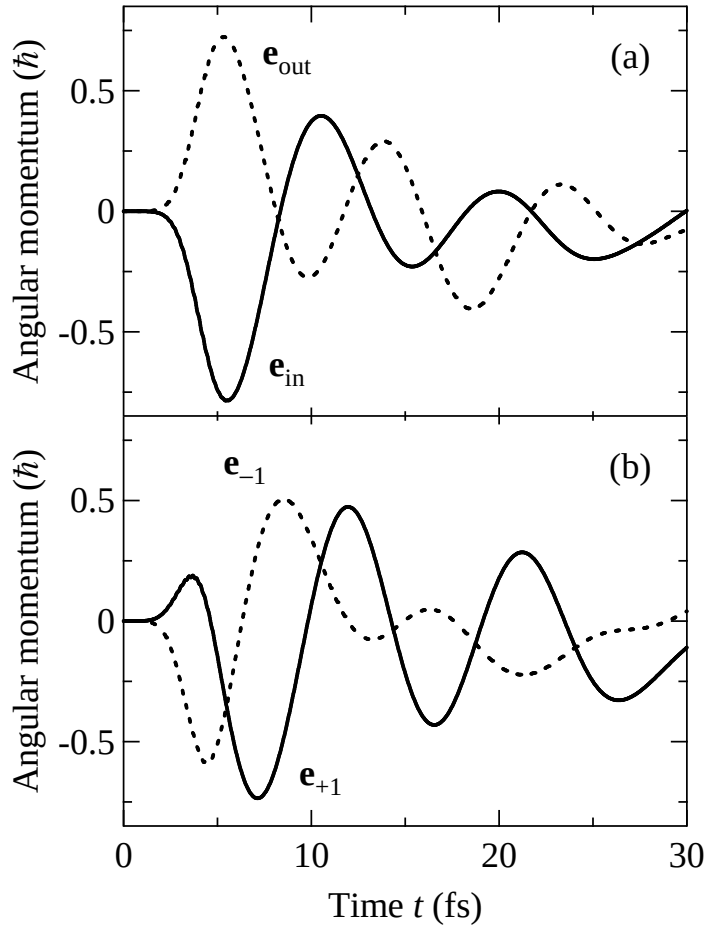

FIG. 7: Expectation value of the electronic angular momentum $L_z(t)$ in DCP irradiated by (a) linearly and (b) circularly polarized UV laser pulses calculated from nuclear WP simulations. In panel (a), the expectation values for $\mathbf{e}_{in}$ and $\mathbf{e}_{out}$ excitations are denoted by the solid and dotted lines, respectively; in panel (b), those for $\mathbf{e}_{+1}$ and $\mathbf{e}_{-1}$ excitations are denoted by the solid and dotted lines, respectively. The laser pulses fully decay at $t = 7.26$ fs.

for its smaller amplitude due to the less efficiency of excitation and the coordinate dependence of $\Lambda(\mathbf{Q})$ defined by Eq. (56). Then, the amplitude of $L_z(t)$ is reduced gradually, which is a characteristic feature absent in the frozen-nuclei model. The reduction in the angular momentum is attributed to two factors: decrease of the overlap between the WPs moving on the relevant two adiabatic PESs, which is observed even within the Born-Oppenheimer approximation (BOA) [64], and electronic relaxation due to nonadiabatic couplings shown in Fig. 6, which is the major factor. The angular-momentum expectation value $L_z(t)$ can

be expressed using the WPs $\psi_L(\mathbf{Q},t)$ and $\psi_H(\mathbf{Q},t)$ as

$$L_z(t) = 2\int d\mathbf{Q}\mathrm{Im}\left[\psi_L^*(\mathbf{Q},t)\,\psi_H(\mathbf{Q},t)\right]\Lambda(\mathbf{Q}). \tag{66}$$

Both of the two factors cause the loss of a superposition of $|L\rangle$ and $|H\rangle$, that is, $\psi_L^*(\mathbf{Q},t)\,\psi_H(\mathbf{Q},t) \to 0$. The oscillatory curves of $L_z(t)$ for $\mathbf{e}_{in}$ and $\mathbf{e}_{+1}$ excitations can be approximated by a sinusoidal exponential decay. The lifetime of the decay is ~ 6 fs for $\mathbf{e}_{in}$ and ~ 18 fs for $\mathbf{e}_{+1}$, of which difference originates from the different rates of nonadiabatic transition in Figs. 6(a) and 6(c). On the other hand, the amplitudes of $L_z(t)$ for $\mathbf{e}_{out}$ and $\mathbf{e}_{-1}$ excitations do not undergo a monotonic decrease but make a small transient recovery (around $t \sim$ 14–20 fs for $\mathbf{e}_{out}$ and $t \sim$ 18–24 fs for $\mathbf{e}_{-1}$). This recovery arises from the regeneration of the superposition of $|L\rangle$ and $|H\rangle$ due to the upward population transfer in the respective time ranges in Figs. 6(b) and 6(d). A little difference in the oscillation period among the four types of excitations stems from the fact that the energy difference between the two adiabatic PESs in the regions where the WPs run depends on the type of excitation. It turned out from the results in Fig. 7 that π-electron rotation controlled by the polarization of a laser pulse is attenuated on the timescale of several tens of femtoseconds by nonadiabatic couplings.

Figure 8 depicts the expectation value of the normal coordinates $\mathbf{Q}(t) \equiv \left\langle \Psi(t) \left| \hat{\mathbf{Q}} \right| \Psi(t) \right\rangle$ with $\hat{\mathbf{Q}}$ being the operator of $\mathbf{Q}$. In Fig. 8(a), the behaviors of $\mathbf{Q}(t)$ triggered by linearly polarized laser pulses are remarkably dependent on the polarization direction: The vibrational amplitude for $\mathbf{e}_{out}$ excitation is more than two-times larger than that for $\mathbf{e}_{in}$ excitation. Contrary to this, in Fig. 8(b), the vibration of DCP differs only slightly between circular polarizations $\mathbf{e}_{+1}$ and $\mathbf{e}_{-1}$, and the trajectories of $\mathbf{Q}(t)$ are located between those for linear ones. These findings are reinforced by vibrational spectral analysis. The frequency spectrum of the WP on the lower PES, $\psi_L(\mathbf{Q},t)$, after the nonadiabatic transition from $|H\rangle$ to $|L\rangle$ is given by the Fourier transform of its autocorrelation function [65]:

$$\sigma_L(\omega) \equiv \mathrm{Re}\int_{t_i}^{t_f} dt e^{(i\omega - 1/\tau)(t-t_i)} \int d\mathbf{Q}\psi_L^*(\mathbf{Q},t_i)\,\psi_L(\mathbf{Q},t). \tag{67}$$

The parameter τ was introduced to smooth the spectra and set at 39.6 fs, which is longer than the vibrational periods of the breathing and distortion modes (28.8 and 21.2 fs). The values of t_i for $\mathbf{e}_{in}$, $\mathbf{e}_{out}$, $\mathbf{e}_{+1}$, and $\mathbf{e}_{-1}$ excitations were 14.0, 10.0, 34.0, and 13.0 fs, respectively, and $t_f - t_i = 99.1$ fs for all of them. The zero of ω was chosen to be the minimum of the lower PES.

Figure 9 displays the frequency spectra for the four types of excitations. For $\mathbf{e}_{in}$ excitation, the maximum value of $\sigma_L(\omega)$ is located at $\tilde{\nu} \sim 1400$ cm^{-1} and another peak appears at $\tilde{\nu} \sim 2500$ cm^{-1} in Fig. 9(a); for $\mathbf{e}_{out}$ excitation, the strongest peak of $\sigma_L(\omega)$ is found at $\tilde{\nu} \sim 2500$ cm^{-1} and besides a couple of strong peaks are exhibited at $\tilde{\nu} > 3000$ cm^{-1}. The wave numbers of 1400, 2500, and 3000 cm^{-1} are almost identical to those of the lowest three vibrational states $(v_b, v_d) = (0, 0)$, (1, 0), and (0, 1) in $|G\rangle$ owing to the

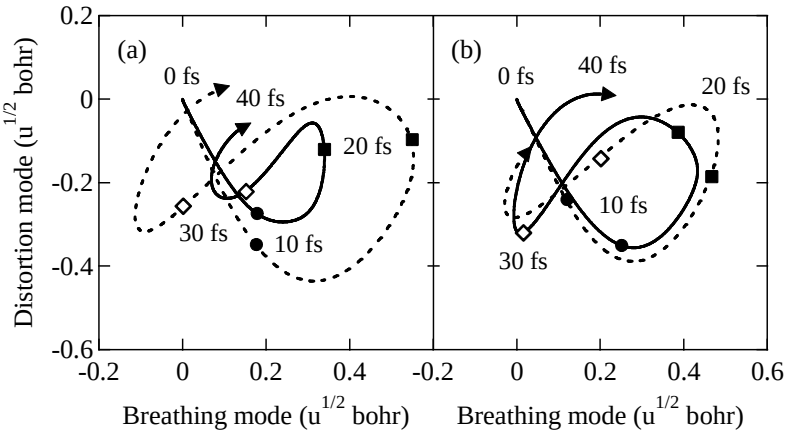

FIG. 8: Expectation value of the normal coordinates $\mathbf{Q}(t)$ of the breathing and distortion modes in DCP irradiated by (a) linearly and (b) circularly polarized UV laser pulses. In panel (a), the expectation values for $\mathbf{e}_{in}$ and $\mathbf{e}_{out}$ excitations are denoted by the solid and dotted lines, respectively; in panel (b), those for $\mathbf{e}_{+1}$ and $\mathbf{e}_{-1}$ excitations are denoted by the solid and dotted lines, respectively. The laser pulses fully decay at $t = 7.26$ fs.

analogy between $|G\rangle$ and $|L\rangle$ in the PES around its minimum. The frequency spectra for linear polarizations in Fig. 9(a) support that at $t > t_i$, $\psi_L(\mathbf{Q}, t)$ is mainly composed of low (high) vibrational quantum states for $\mathbf{e}_{in}$ ($\mathbf{e}_{out}$) excitation. In marked distinction from linear polarizations, the spectral features for circular ones in Fig. 9(b) are very similar to each other: The primary peaks of $\sigma_L(\omega)$ for $\mathbf{e}_{+1}$ and $\mathbf{e}_{-1}$ excitations are both at $\tilde{\nu} \sim 1400$ cm^{-1}, while the intensities of the other peaks are a little stronger for the latter. This obviously indicates that $\psi_L(\mathbf{Q}, t)$ contains the same frequency components for left and right circular polarizations after the nonadiabatic transition.

The striking difference in the vibrational amplitude between $\mathbf{e}_{in}$ and $\mathbf{e}_{out}$ excitations suggests that ultrafast π-electron dynamics in aromatic molecules such as DCP for linear polarizations can be distinguished experimentally by vibrational spectroscopy in the frequency domain without time-resolved measurements. This idea may be utilized for rapid identification of molecular chirality since the rotation direction of π electrons basically differs between enantiomers according to their alignments with respect to the linear polarization direction.

IV-5. Comparison to the Born-Oppenheimer Approximation

We also carried out nuclear WP simulations under the BOA by solving Eq. (62) without the nonadiabatic terms $G_{nn'}(\mathbf{Q})$. The procedure of numerical integration was the same as described in Section IV-2. In this approximation, the nonadiabatic coupling between the quasi-degenerate states was completely neglected and thereby the WPs simply propagated on the individual PESs. As seen in Fig. 10, the phase in the oscillation of angular momentum is dependent on laser polarization in this case as well. However, other features

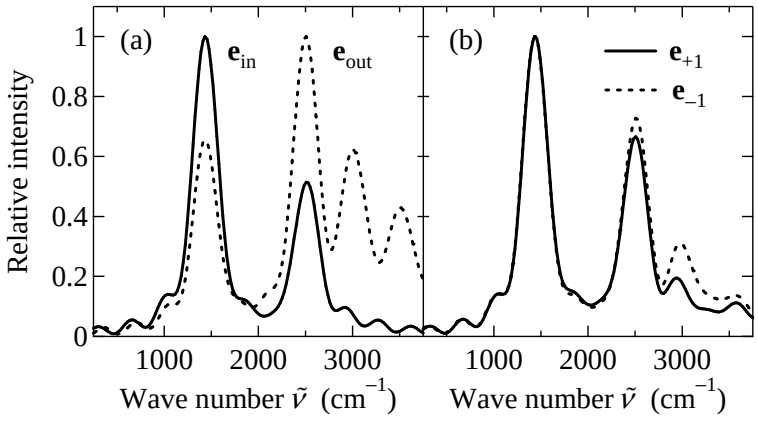

FIG. 9: The frequency spectra of $\psi_L(\mathbf{Q}, t)$, $\sigma_L(\omega)$, defined by Eq. (67) for DCP irradiated by (a) linearly and (b) circularly polarized UV laser pulses. In panel (a), the spectra for $\mathbf{e}_{in}$ and $\mathbf{e}_{out}$ excitations are denoted by the solid and dotted lines, respectively; in panel (b), those for $\mathbf{e}_{+1}$ and $\mathbf{e}_{-1}$ excitations are denoted by the solid and dotted lines, respectively. In each case, the values of $\sigma_L(\omega)$ were scaled so that the maximum value is unity.

in Figs. 7 and 8 which are deemed to be caused by nonadiabatic couplings disappear under the BOA as expected: The amplitude of $L_z(t)$ does not decay exponentially but exhibits periodic reduction and recovery in turn owing to the temporal change in the WP overlap. The trajectory of $\mathbf{Q}(t)$ in Fig. 11 hardly depends on the type of excitation and the vibrational amplitude is larger than that for $\mathbf{e}_{in}$ excitation in Fig. 8(a) but smaller than those for circular polarizations in Fig. 8(b). These facts corroborate that the laser-polarization effects on nonadiabatic transition indeed give birth to the polarization-dependent behaviors in π-electron rotation and molecular vibration such as the decay of angular momentum with different lifetimes.

IV-6. Wave Packet Interference

Figures 12 and 13 illustrate the propagations of the WPs on the relevant two adiabatic PESs to take a close look at the laser-polarization effects on nonadiabatic transition. For both linear and circular polarizations, the probability densities $|\psi_L(\mathbf{Q}, t)|^2$ and $|\psi_H(\mathbf{Q}, t)|^2$ created in the two excited states at $t \sim 5$ fs resemble that of the initial WP $|\psi_G(\mathbf{Q}, 0)|^2$, and then the WPs start to move along the gradient of each PES. Yet, when the WPs approach the avoided crossing, the nonadiabatic nature of vibronic dynamics in this system emerges differently for the four types of excitations. For $\mathbf{e}_{in}$ excitation, the WP on the higher PES is diminished by nonadiabatic transition at $t \sim 12$ fs and the contour map of $|\psi_L(\mathbf{Q}, t)|^2$ clearly displays the node originating from the interference which is represented by the broken line in Fig. 12(a); thereafter, the WPs on the two adiabatic PESs are deformed largely. In contrast, the WPs for $\mathbf{e}_{out}$ excitation in Fig. 12(b) maintain a Gaussian-like form even after the nonadiabatic transition which is already in progress at $t \sim 8$ fs.

For circular polarizations, the WPs on the two PESs behave as expected from the

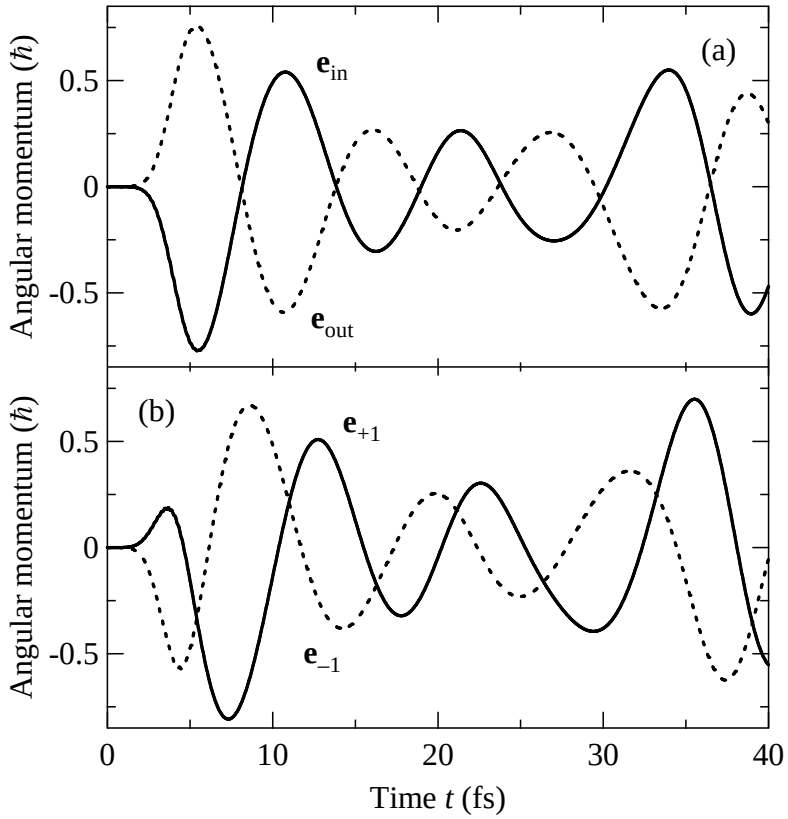

FIG. 10: Expectation value of the electronic angular momentum $L_z(t)$ in DCP irradiated by (a) linearly and (b) circularly polarized UV laser pulses calculated from nuclear WP simulations under the BOA. In panel (a), the expectation values for $\mathbf{e}_{in}$ and $\mathbf{e}_{out}$ excitations are denoted by the solid and dotted lines, respectively; in panel (b), those for $\mathbf{e}_{+1}$ and $\mathbf{e}_{-1}$ excitations are denoted by the solid and dotted lines, respectively. The laser pulses fully decay at $t = 7.26$ fs.

tendencies of the populations in Figs. 6(c) and 6(d). In Fig. 13(a), only a small fraction of $\psi_H(\mathbf{Q}, t)$ has been transferred to $|L\rangle$ until $t \sim 12$ fs and there is no interference pattern in the WPs for $\mathbf{e}_{+1}$ excitation. The WPs for $\mathbf{e}_{-1}$ excitation in Fig. 13(b) have intermediate features between those for $\mathbf{e}_{in}$ and $\mathbf{e}_{out}$ excitations: No clear interference is observed in the WPs but the shape of $|\psi_L(\mathbf{Q}, t)|^2$ is distorted from a Gaussian especially at $t \sim 12$ fs. As a consequence of nonadiabatic couplings, the center of $\psi_L(\mathbf{Q}, t)$, which contributes dominantly to $\mathbf{Q}(t)$ in Fig. 8, proceeds in a low-energy (high-energy) region on the lower PES for $\mathbf{e}_{in}$ ($\mathbf{e}_{out}$) excitation, whereas the motions of the center for circular polarizations are analogous to each other.

The laser-polarization effects on the populations $P_L(t)$ and $P_H(t)$, expectation values $L_z(t)$ and $\mathbf{Q}(t)$, and WPs $\psi_L(\mathbf{Q}, t)$ and $\psi_H(\mathbf{Q}, t)$ can be interpreted in terms of interferences between the WP existing on the original PES and that created by nonadiabatic couplings. First, we take the case of $\mathbf{e}_{out}$ excitation. As mentioned in the model analysis in Section III,

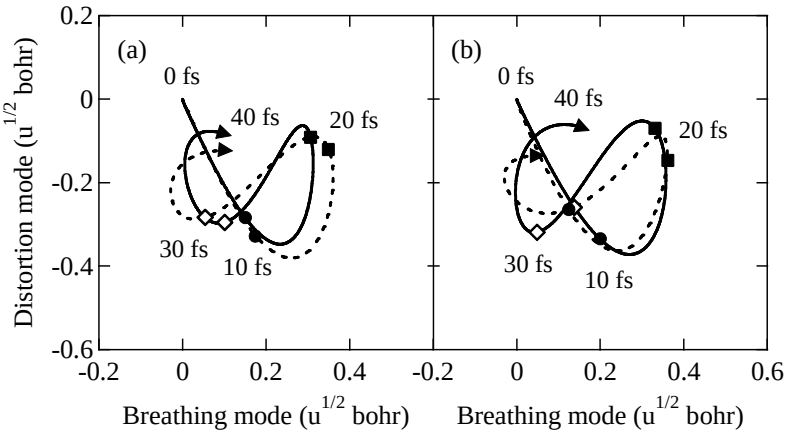

FIG. 11: Expectation value of the normal coordinates $\mathbf{Q}(t)$ of the breathing and distortion modes in DCP irradiated by (a) linearly and (b) circularly polarized UV laser pulses under the BOA. In panel (a), the expectation values for $\mathbf{e}_{in}$ and $\mathbf{e}_{out}$ excitations are denoted by the solid and dotted lines, respectively; in panel (b), those for $\mathbf{e}_{+1}$ and $\mathbf{e}_{-1}$ excitations are denoted by the solid and dotted lines, respectively. The laser pulses fully decay at $t = 7.26$ fs.

a linearly polarized laser pulse with $\mathbf{e}_{out}$ achieves $\theta = \pi$; in other words, it initially produces a linear combination of $\psi_L(\mathbf{Q}, t)$ and $\psi_H(\mathbf{Q}, t)$ out of phase in aromatic molecules. Then, their relative quantum phase evolves during irradiation [by $-\vartheta(t)$ in the cases of rectangular-envelope pulses as in Eq. (51)] and also gains a dynamical phase associated with the shape of each PES as the WPs propagate. In nonadiabatic transition, an additional phase shift is further imposed on the WP created by nonadiabatic couplings, which interferes with that on the other PES. We do not quantify the additional phase in DCP, but the downward population transfer around $t \sim 5$–10 fs in Fig. 6(b) implies opposite interferences on the two PESs: The WPs are almost in phase after the nonadiabatic transition from $|H\rangle$ to $|L\rangle$ and interfere constructively on the lower PES, while those after the transition from $|L\rangle$ to $|H\rangle$ are out of phase with destructive interference on the higher PES. The constructive interference on the lower PES works particularly on high vibrational quantum states in $\psi_L(\mathbf{Q}, t)$, yielding the strong peaks of $\sigma_L(\omega)$ at $\tilde{\nu} \sim 2500$ cm^{-1} and $\tilde{\nu} > 3000$ cm^{-1} in Fig. 9(a). The direction of the population transfer flips as the relative quantum phase develops as in Fig. 6(b).

Next, for $\mathbf{e}_{in}$ excitation in which the two initially prepared WPs are in phase ($\theta = 0$), the interference effects are reversed from those for $\mathbf{e}_{out}$ excitation: For DCP, the interference is destructive on the lower PES but constructive on the higher one around $t \sim 5$–10 fs. The amount of the WP created by the nonadiabatic transition from $|L\rangle$ to $|H\rangle$, which interferes with $\psi_H(\mathbf{Q}, t)$, is less than that for the transition from $|H\rangle$ to $|L\rangle$, which interferes with $\psi_L(\mathbf{Q}, t)$; this is the reason why the resultant upward population transfer around $t \sim 5$–10 fs in Fig. 6(a) is small. The WPs on the two PESs then reach the avoided crossing and the reverse population transfer takes place around $t \sim 10$–14 fs. The interference enhances low

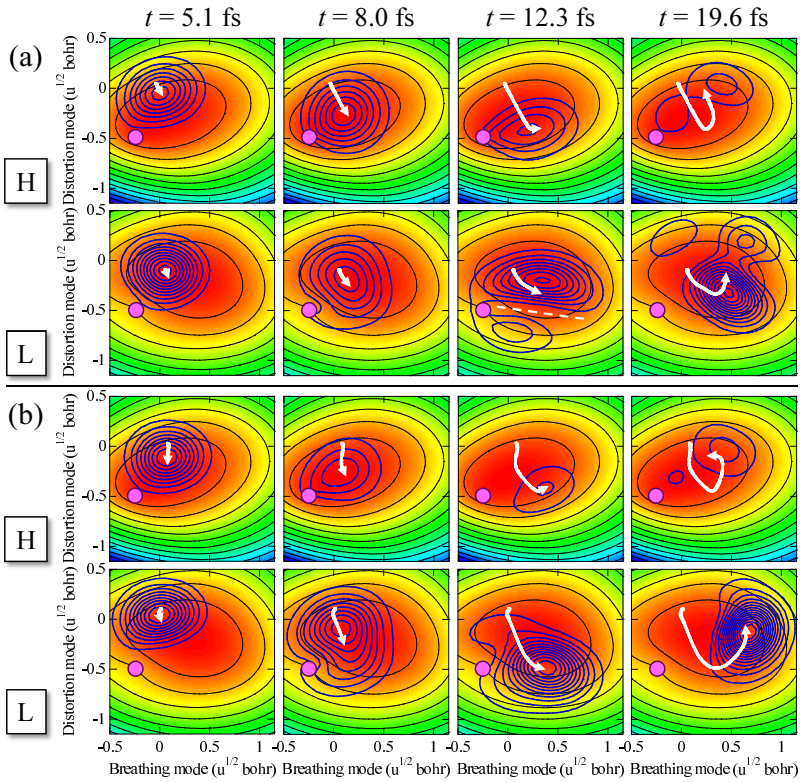

FIG. 12: Propagation of the adiabatic WPs on the two-dimensional adiabatic PESs of $|L\rangle$ and $|H\rangle$ for (a) $\mathbf{e}_{in}$ and (b) $\mathbf{e}_{out}$ excitations. The origin of the PESs is the optimized geometry of $|G\rangle$ and the avoided crossing is designated by a circle. The bold contours represent the probability densities $|\psi_L(\mathbf{Q},t)|^2$ and $|\psi_H(\mathbf{Q},t)|^2$. The arrows indicate the motion of the center of the WPs. In panel (a), the node in $\psi_L(\mathbf{Q}, 12.3\text{ fs})$ is represented by the broken line.

vibrational quantum states in $\psi_L(\mathbf{Q},t)$, increasing the probability density in a low-energy region on the lower PES as seen in Fig. 12(a).

In the cases of circular polarizations, $\psi_L(\mathbf{Q},t)$ and $\psi_H(\mathbf{Q},t)$ are initially neither in phase nor out of phase because $\theta = \pm(\chi_H - \chi_L)$ for $\mathbf{e}_{\pm1}$; for DCP, $\theta = \pm 0.35\pi$. Hence, no fully constructive or destructive interference occurs on either PES at $t \sim 5$–10 fs, resulting in the vibrational amplitudes in Fig. 8(b) which are intermediate between those for linear polarizations in Fig. 8(a). As the relative quantum phase between the WPs evolves in the negative direction, for $\mathbf{e}_{-1}$ excitation with $\theta = -0.35\pi$, it takes more time than for $\mathbf{e}_{out}$ with $\theta = \pi$ but less time than for $\mathbf{e}_{in}$ with $\theta = 0$ to experience constructive and destructive interferences on the lower and higher PESs, respectively. Consequently, the downward population transfer for $\mathbf{e}_{-1}$ excitation appears at $t \sim 8$–13 fs in Fig. 6(d). For $\mathbf{e}_{+1}$ excitation with $\theta = 0.35\pi$, the WPs pass through the avoided crossing before matching the requirement of interference for population transfer and thus the nonadiabatic transition is unfinished until they come closer again to the avoided crossing at $t \sim 30$ fs as in Fig. 6(c).

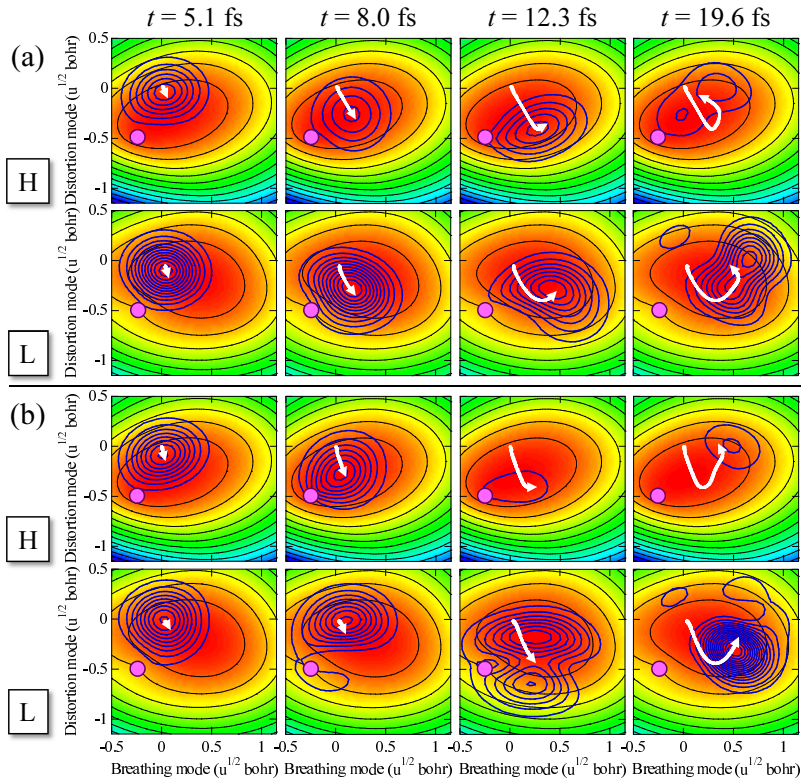

FIG. 13: Propagation of the adiabatic WPs on the two-dimensional adiabatic PESs of $|L\rangle$ and $|H\rangle$ for (a) $\mathbf{e}_{+1}$ and (b) $\mathbf{e}_{-1}$ excitations. The origin of the PESs is the optimized geometry of $|G\rangle$ and the avoided crossing is designated by a circle. The bold contours represent the probability densities $|\psi_L(\mathbf{Q},t)|^2$ and $|\psi_H(\mathbf{Q},t)|^2$. The arrows indicate the motion of the center of the WPs.

The nuclear WP simulations in this section demonstrated that the initial relative phase θ between the WPs of the quasi-degenerate excited states, which is determined by the ellipticity angle β and orientation angle δ of the incident light, governs not only electron ring currents but also the subsequent molecular vibration through nonadiabatic couplings. What is more, we can also manipulate the time-dependent phase due to irradiation, namely, $\vartheta(t)$ by tuning the other laser parameters such as the peak field strength ε_p and pulse duration t_d. This suggests that by applying a laser pulse of arbitrary polarization, in principle, it is possible to produce a superposition of the quasi-degenerate states with an arbitrary relative phase. Ultimately, the interference between nuclear WPs in nonadiabatic transition can be controlled as desired by means of attosecond/several-femtosecond laser pulses, leading to sophisticated control of molecular vibrations.

V. CONCLUSIONS

We have reviewed our recent studies on the nonadiabatically coupled vibronic dynamics of aromatic molecules with quasi-degenerate π-electronic states excited by an ultrashort UV laser pulse of arbitrary polarization. First, the concept of electronic angular momentum eigenstates in aromatic molecules was introduced to quantify laser-driven π-electron rotation (ring current) in reference to MO theory. Next, for the purpose of analyzing the role of laser polarization in the optical excitation process, we employed the V-type three-level model under the frozen-nuclei condition and derived general formulations of the coherent electronic WP and angular-momentum expectation value in both degenerate and quasi-degenerate systems. The initial relative phase between the quasi-degenerate excited states, θ, is determined by the ellipticity angle β and orientation angle δ of an applied laser field, and the relation among the three variables was provided in Eq. (27). The time-dependent part of the relative quantum phase, $\vartheta(t)$, is adjustable by the laser pulse as well. A desired superposition of the quasi-degenerate states can therefore be created by applying ultrashort laser pulses. The angular-momentum expectation value follows the temporal behavior in the relative quantum phase as shown in Eq. (55) and oscillates after irradiation with the period corresponding to the energy gap between the quasi-degenerate states. The numerical results of electronic WP simulations for a model system of DCP confirmed the controllability of the phase in the oscillation of angular momentum.

Nuclear WP simulations were also carried out on effective PESs of DCP. By nonadiabatic couplings with molecular vibrations, the angular momentum of π electrons decays on the timescale of several tens of femtoseconds. The comparison in the expectation values of vibrational coordinates between the linear and circular polarization cases revealed an interesting finding: The amplitude of the molecular vibration coupled to π-electron rotation is prominently dependent on the orientation of linear polarization vectors, while it is almost the same for left and right circular polarizations. This characteristic dependence of vibrational amplitudes on laser polarization is ascribed to the interference effects in nonadiabatic transition dictated by the relative quantum phase between the WPs. These results suggest the potential application of attosecond/several-femtosecond polarized laser pulses as a promising tool to control molecular vibrations through the WP interference in nonadiabatic transition.

In this article, we focused on ultrafast π-electron rotation and vibronically coupled molecular vibrations induced by a single-color laser. If a two-color laser is employed, another controlling factor of coherent vibronic dynamics is the relative optical phase between different frequency components [43, 45]. Very recently, the scheme for optical generation of π-electron rotation has been extended to a nonplanar system [66, 67]. We expect that the knowledge obtained for aromatic molecules serves as a basis for studying more complicated polarization-dependent dynamics in larger systems, e.g., intense-field fragmentation of C_{60} [30]. Control of nonadiabatic vibrational/fragmentation dynamics induced by multiphoton electronic excitation is a worthwhile subject for future research.

Acknowledgements

This work was supported in part by JSPS Research Grants (No. 23550003, No. 23750003, and No. 24245001).

References

[1] F. Lépine, G. Sansone, and M. J. J. Vrakking, Chem. Phys. Lett. **578**, 1 (2013).
[2] Y. Arasaki, K. Takatsuka, K. Wang, and V. McKoy, J. Chem. Phys. **132**, 124307 (2010); Y. Arasaki, K. Wang, V. McKoy, and K. Takatsuka, Phys. Chem. Chem. Phys. **13**, 8681 (2011); Y. Arasaki, K. Wang, V. McKoy, and K. Takatsuka, J. Phys. B **45**, 194006 (2012).
[3] C. Z. Bisgaard *et al.*, Science **323**, 1464 (2009); P. Hockett, C. Z. Bisgaard, O. J. Clarkin, and A. Stolow, Nature Phys. **7**, 612 (2011).
[4] Y. Suzuki, M. Stener, and T. Seideman, Phys. Rev. Lett. **89**, 233002 (2002); J. Chem. Phys. **118**, 4432 (2003).
[5] T. Horio, T. Fuji, Y. Suzuki, and T. Suzuki, J. Am. Chem. Soc. **131**, 10392 (2009); S. Y. Liu *et al.*, Phys. Rev. A **81**, 031403(R) (2010).
[6] T. Fuji *et al.*, J. Chem. Phys. **133**, 234303 (2010).
[7] B. Abulimiti *et al.*, J. Chem. Phys. **134**, 234301 (2011).
[8] C. M. Dion *et al.*, Chem. Phys. Lett. **302**, 215 (1999).
[9] H. Sakai *et al.*, J. Chem. Phys. **110**, 10235 (1999); J. J. Larsen, H. Sakai, C. P. Safvan, I. Wendt-Larsen, and H. Stapelfeldt, J. Chem. Phys. **111**, 7774 (1999).
[10] J. J. Larsen, K. Hald, N. Bjerre, H. Stapelfeldt, and T. Seideman, Phys. Rev. Lett. **85**, 2470 (2000).
[11] K. Hoki and Y. Fujimura, Chem. Phys. **267**, 187 (2001).
[12] H. Stapelfeldt and T. Seideman, Rev. Mod. Phys. **75**, 543 (2003).
[13] K. Nakagami, Y. Mizumoto, and Y. Ohtsuki, J. Chem. Phys. **129**, 194103 (2008); H. Abe and Y. Ohtsuki, Phys. Rev. A **83**, 053410 (2011); Chem. Phys. **400**, 13 (2012).
[14] H. Sakai, S. Minemoto, H. Nanjo, H. Tanji, and T. Suzuki, Phys. Rev. Lett. **90**, 083001 (2003); S. Minemoto, H. Nanjo, H. Tanji, T. Suzuki, and H. Sakai, J. Chem. Phys. **118**, 4052 (2003).
[15] H. Tanji, S. Minemoto, and H. Sakai, Phys. Rev. A **72**, 063401 (2005).
[16] N. Takemoto and K. Yamanouchi, Chem. Phys. Lett. **451**, 1 (2008).
[17] K. Nakajima, H. Abe, and Y. Ohtsuki, J. Phys. Chem. A **116**, 11219 (2012).
[18] T. Seideman, Phys. Rev. Lett. **83**, 4971 (1999).
[19] F. Rosca-Pruna and M. J. J. Vrakking, Phys. Rev. Lett. **87**, 153902 (2001); J. Chem. Phys. **116**, 6567 (2002).
[20] V. Renard *et al.*, Phys. Rev. Lett. **90**, 153601 (2003).
[21] P. W. Dooley *et al.*, Phys. Rev. A **68**, 023406 (2003).
[22] E. Péronne, M. D. Poulsen, C. Z. Bisgaard, and H. Stapelfeldt, Phys. Rev. Lett. **91**, 043003 (2003); C. Z. Bisgaard, M. D. Poulsen, E. Péronne, S. S. Viftrup, and H. Stapelfeldt, Phys. Rev. Lett. **92**, 173004 (2004); M. D. Poulsen *et al.*, J. Chem. Phys. **121**, 783 (2004); E. Péronne *et al.*, Phys. Rev. A **70**, 063410 (2004).
[23] E. Hamilton *et al.*, Phys. Rev. A **72**, 043402 (2005).
[24] T. Kanai, S. Minemoto, and H. Sakai, Nature **435**, 470 (2005).
[25] W. Boutu *et al.*, Nature Phys. **4**, 545 (2008).
[26] B. K. McFarland, J. P. Farrell, P. H. Bucksbaum, and M. Gühr, Science **322**, 1232 (2008).

[27] J. Itatani *et al.*, Nature **432**, 867 (2004).
[28] S. Haessler *et al.*, Nature Phys. **6**, 200 (2010).
[29] C. Vozzi *et al.*, Nature Phys. **7**, 822 (2011).
[30] I. V. Hertel *et al.*, Phys. Rev. Lett. **102**, 023003 (2009); I. Shchatsinin, H.-H. Ritze, C. P. Schulz, and I. V. Hertel, Phys. Rev. A **79**, 053414 (2009).
[31] I. Barth and J. Manz, Angew. Chem. **118**, 3028 (2006); Angew. Chem. Int. Ed. **45**, 2962 (2006); I. Barth, J. Manz, Y. Shigeta, and K. Yagi, J. Am. Chem. Soc. **128**, 7043 (2006); I. Barth and J. Manz, in *Progress in Ultrafast Intense Laser Science*, edited by K. Yamanouchi, G. Gerber, and A. D. Bandrauk (Springer, Berlin, 2010), Vol. 6, pp. 21-44.
[32] I. Barth, J. Manz, and P. Sebald, Chem. Phys. **346**, 89 (2008).
[33] I. Barth, J. Manz, and L. Serrano-Andrés, Chem. Phys. **347**, 263 (2008).
[34] I. Barth, L. Serrano-Andrés, and T. Seideman, J. Chem. Phys. **129**, 164303 (2008); **130**, 109901 (2009).
[35] T. Yonehara and K. Takatsuka, Chem. Phys. **366**, 115 (2009).
[36] K. Takatsuka and T. Yonehara, Phys. Chem. Chem. Phys. **13**, 4987 (2011).
[37] J. J. Rodriguez, and S. Mukamel, J. Phys. Chem. A **116**, 11095 (2012).
[38] O. E. Alon, V. Averbukh, and N. Moiseyev, Phys. Rev. Lett. **80**, 3743 (1998); R. Baer, D. Neuhauser, P. R. Ždánská, and N. Moiseyev, Phys. Rev. A **68**, 043406 (2003).
[39] F. Ceccherini and D. Bauer, Phys. Rev. A **64**, 033423 (2001); F. Ceccherini, D. Bauer and F. Cornolti, J. Phys. B **34**, 5017 (2001).
[40] K. Nobusada and K. Yabana, Phys. Rev. A **75**, 032518 (2007).
[41] I. S. Ulusoy and M. Nest, J. Am. Chem. Soc. **133**, 20230 (2011).
[42] M. Kanno, H. Kono, and Y. Fujimura, Angew. Chem. **118**, 8163 (2006); Angew. Chem. Int. Ed. **45**, 7995 (2006).
[43] M. Kanno, K. Hoki, H. Kono, and Y. Fujimura, J. Chem. Phys. **127**, 204314 (2007).
[44] M. Kanno, H. Kono, Y. Fujimura, and S. H. Lin, Phys. Rev. Lett. **104**, 108302 (2010).
[45] M. Kanno, H. Kono, and Y. Fujimura, in *Progress in Ultrafast Intense Laser Science*, edited by K. Yamanouchi, D. Charalambidis, and D. Normand (Springer, Berlin, 2011), Vol. 7, pp. 53-78.
[46] H. Mineo *et al.*, Chem. Phys. **392**, 136 (2012).
[47] M. Kanno, H. Kono, S. H. Lin, and Y. Fujimura, in *Quantum Systems in Chemistry and Physics: Progress in Methods and Applications*, edited by K. Nishikawa, J. Maruani, E. J. Brändas, G. Delgado-Barrio, and P. Piecuch (Springer, Netherlands, 2012), Progress in Theoretical Chemistry and Physics Vol. 26, pp. 121-148.
[48] M. Kanno, Y. Ono, H. Kono, and Y. Fujimura, J. Phys. Chem. A **116**, 11260 (2012).
[49] L. Salem, *The Molecular Orbital Theory of Conjugated Systems* (Benjamin, New York, 1966), pp. 112-116.
[50] A. A. Frost and B. Musulin, J. Chem. Phys. **21**, 572 (1953).
[51] M. Rubio, B. O. Ross, L. Serrano-Andrés, and M. Merchán, J. Chem. Phys. **110**, 7202 (1999).
[52] D. Sundholm, Chem. Phys. Lett. **317**, 392 (2000).
[53] (a) B. W. Shore, *The Theory of Coherent Atomic Excitation* (Wiley, New York, 1990), Vol. 2, pp. 778-787; (b) Vol. 1, pp. 235-239; (c) Vol. 1, pp. 304-309.
[54] R. Selle *et al.*, Opt. Lett. **33**, 803 (2008); P. Nuernberger *et al.*, J. Opt. A **11**, 085202 (2009).
[55] M. T. Seidel, Z. Zhang, S. Yan, and H.-S. Tan, J. Opt. Soc. Am. B **28**, 1146 (2011); M. T. Seidel, Z. Zhang, S. Yan, K. L. Wells, and H.-S. Tan, J. Opt. Soc. Am. B **28**, 2718 (2011).
[56] K.-J. Yuan and A. D. Bandrauk, J. Phys. B **45**, 074001 (2012).
[57] I. N. Levine, *Quantum Chemistry* (Prentice Hall, New Jersey, 2009), 6th ed., pp. 471-635.
[58] H.-J. Werner *et al.*, MOLPRO, version 2006.1, (Cardiff, UK, 2006).

[59] Y. Ohtsuki, K. Nakagami, and Y. Fujimura, in *Advances in Multi-Photon Processes and Spectroscopy*, edited by S. H. Lin, A. A. Villaeys, and Y. Fujimura (World Scientific, Singapore, 2001), Vol. 13, pp. 1-127.
[60] M. Baer, *Beyond Born-Oppenheimer* (Wiley, Hoboken, New Jersey, 2006), pp. 26-57.
[61] B. Sarkar and S. Adhikari, Int. J. Quant. Chem. **109**, 650 (2009).
[62] D. Simah, B. Hartke, and H.-J. Werner, J. Chem. Phys. **111**, 4523 (1999).
[63] P. Gross, D. Neuhauser, and H. Rabitz, J. Chem. Phys. **96**, 2834 (1992).
[64] M. Born and J. R. Oppenheimer, Ann. Phys. **84**, 457 (1927).
[65] D. J. Tannor, *Introduction to Quantum Mechanics: A Time-Dependent Perspective* (University Science Books, California, 2007), pp. 81-86.
[66] H. Mineo *et al.*, J. Am. Chem. Soc. **134**, 14279 (2012).
[67] H. Mineo, S. H. Lin, and Y. Fujimura, J. Chem. Phys. **138**, 074304 (2013).